ELSEVIER

Contents lists available at ScienceDirect

Journal of Non-Crystalline Solids

journal homepage: www.elsevier.com/locate/jnoncrysol



Viscosity of melts in the NaAlSiO₄-KAlSiO₄-SiO₂ system: Configurational entropy modelling



Geneviève Robert^{a,*}, Rebecca A. Smith^{a,1}, Alan G. Whittington^{b,c}

- ^a Department of Geology, Bates College, Lewiston, ME 04240, USA
- b Department of Geological Sciences, University of Missouri, Columbia, MO 65211, USA
- ^c Department of Geological Sciences, The University of Texas at San Antonio, San Antonio, TX 78249, USA

ARTICLE INFO

Keywords: Viscosity Aluminosilicate melts Alkali mixing Configurational entropy modelling

ABSTRACT

We provide new viscosity data in the system SiO_2 -(Na,K)AlSiO₄, for the nepheline-kalsilite and jadeite-leucite joins. We present a configurational entropy model for the viscosity of melts in the system as a function of Na/(Na + K) and Al/(Al + Si) ratios. Our modelling indicates that: i) Viscosity data are reproduced well by a non-ideal, symmetrical form of the parameters $S^{conf}(T_g)$ and B_e , ii) Na-K mixing is the main source of additional entropy in the system based on the limited dependence of $S^{conf}(T_g)$ and B_e parameters on Al/(Al + Si) ratio, iii) A_e likely varies as a function of Al/(Al + Si) ratio. Melt fragility in the system increases with increasing Al/(Al + Si) ratio and is greater for Na or K end-member melts than mixed melts. The viscosity of nominally fully-polymerized melts in the SiO_2 -(Na,K)AlSiO₄ system can be modelled through chemical mixing, without explicit consideration of the important changes in structure related to changes in K/(Na + K) and Al/(Al + Si) ratios.

1. Introduction

The nepheline-kalsilite-quartz system (Fig. 1) contains a number of important compositions for modelling magmatic systems, and offers an ideal analog system for the study of mixed-alkali melts, Na2O and K2O being the most important alkali oxides by weight in magmas. Viscosity studies in the system have largely concentrated on the NaAlO₂-SiO₂ join and the haplogranite subsystem [15,30,34,37,38,40-42], with obvious applications to granites and rhyolites. Le Losq and Neuville [18] investigated Na-K mixing along the silica-rich alkali feldspar and (Na,K)AlSi₅O₁₂ joins and Le Losq et al. [19] investigated compositions along the (Na,K)AlSi_{1.3}O_{4.7} and (Na,K)AlSiO₄ joins. We expand the systematic quantification of the effects of alkali mixing on viscosity to silica-poor aluminosilicate melts, at two different Al/(Al + Si) ratios, specifically along the (Na,K)AlSi₂O₆ and the (Na,K)AlSiO₄ joins (Fig. 1). The metaluminous melts along the $NaAlSi_xO_{2x+2}$ – $KAlSi_xO_{2x+2}$ joins in the nepheline-kalsilite-quartz system have a nominal ratio of nonbridging oxygen to tetrahedrally-coordinated cations (NBO/T) of 0, as each alkali atom charge-balances one tetrahedrally-coordinated aluminum atom, and are nominally fully polymerized. However, the work of Stebbins and Xu [36] suggests the presence of small amounts of nonbridging oxygen atoms (NBOs) in metaluminous (and therefore nominally fully polymerized) glasses; NBOs in metaluminous glasses are also suggested by the presence of a peraluminous viscosity maximum in ${\rm Na_2O\text{-}Al_2O_3\text{-}SiO_2}$ melts instead of the expected metaluminous one [41]. Murdoch et al. [23] demonstrated that smaller, highly-charged cations favor a wider distribution of silicate and aluminate tetrahedra in aluminosilicate melts, that is, they favor more Al-Si disorder in contrast to melts in which the aluminum avoidance principle is strictly observed [21]. It could be expected that with increasing Al/Si ratio, more order is required to satisfy the aluminum avoidance principle [23,40], in these sodium-potassium aluminosilicate melts.

Le Losq and Neuville [18] showed the effects of mixing of Na and K (mixed alkali effect; [6,14]) on the viscosity of silica-rich aluminosilicate melts. Indeed, the potassium and sodium end-members on each join in the system have different viscosities, and the intermediate viscosities are not a simple linear function of Na/K ratio, suggesting changes in structure along each join. Le Losq and Neuville [18] further explored the structural changes that occur as K substitutes for Na by Raman spectroscopy and more recently by molecular dynamics simulations [19]. They suggest, on the basis of their Raman spectroscopy data on silica-rich glasses, that: i) an increase in K relative to Na results in an increase of three- and four- membered rings relative to rings with higher members; ii) an increase in K favors the formation of Si-O-Si-O-Si three-membered rings relative to Si-O-Al-O-Si rings; iii) two populations of six-membered rings distinguished by their intertetrahedral (T-

E-mail address: grobert@bates.edu (G. Robert).

^{*} Corresponding author.

¹ Present address: Department of Geosciences, University of Massachusetts - Amherst, Amherst, MA, 01003, USA.

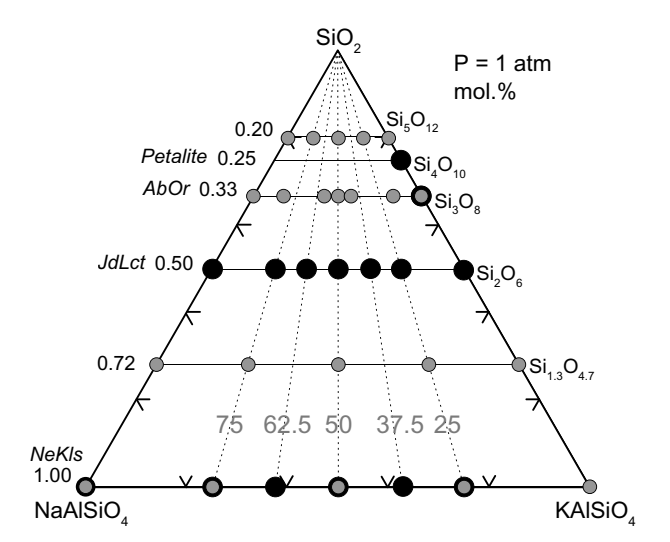


Fig. 1. Black circles: glass and melt compositions from this study. Grey circles: glass and melt compositions studied by Le Losq and Neuville [18] and Le Losq et al. [19]. The Si:O ratio is shown for each join on the right side and the Al/Si ratio is shown on the left side. Not shown are samples studied by Toplis et al. [40], Stein and Spera [37], N'dala et al. [24], Urbain et al. [42], Riebling [30] along the NaAlSiO₄-SiO₂ join, and samples studied by N'dala et al. [24] and Urbain et al. [42] along the KAlSiO₄-SiO₂ join.

O-T) angles may coexist, one of which is suggested to have an evolving T-O-T angle with increasing K whereas the other remains unchanged by the alkali substitution. They attribute the viscosity patterns they observed in the silica-rich melts to these structural changes. They explain the small observed viscosity changes at high Na/K ratios by a predominance of a Si-Al-Na-O subnetwork where K is easily accommodated. At low Na/K ratio, they explain the large viscosity increases they observed by a predominance of a more ordered Si-Al-K-O subnetwork. They explain the slight viscosity decrease relative to the endmembers observed at intermediate Na/K ratios by either a pairing of the Na $^+$ and K $^+$ ions or by a random distribution of the two subnetworks at the medium scale.

Le Losq et al. [19] proposed that the clusters of alkalies (K vs. Na subnetworks) associate with Al-rich regions of the network, violating the Al-avoidance principle, and that this effect is stronger in melts with higher Al/Si ratio. Indeed, their molecular dynamics simulations predict Al-Al to be only ~18% of all inter-tetrahedral distances, consistent with ~13% observed with ¹⁷O MAS NMR [20], which is less than the ~25% expected from a random distribution of the Al in the network. The mixed alkali effect is more important at higher Al/Si ratios, and percolation in alkali channels, as proposed by Greaves [11] and Greaves and Ngai [12] with the Modified Random Network and Compensated Continuous Random Network models for the structure of alkali-rich silicate melts, is only attained in melts with high Al/Si ratios and at high X_K whereas only clusters are found at low Al/Si ratios or low X_K . Le Losq et al. [19] conclude that increasing the proportion of K over Na dilates tetrahedral rings and cages of the network, which shortens and strengthens the Si-O and Al-O bonds, increasing the viscosity of the melt. This strengthening of both Si-O and Al-O bonds allows for more Al-O-Al bonds to be stable in the network.

1.1. The mixed alkali effect and configurational entropy theory

The mixed alkali effect refers to a non-negligible deviation from the simple additivity of physical properties, such as viscosity, upon mixing of alkalies [6,14]. This behavior can be explained in the framework of the configurational entropy theory [26] based on the Adam and Gibbs [1] theory of melt relaxation, where viscosity is expressed as a function of the configurational entropy of melts. The theory assumes that

structural relaxation times are determined by the probability of configurational rearrangements in the melt. The structural relaxation time of a melt (τ) is proportional to the relaxed Newtonian shear viscosity of a melt ($\tau = \frac{\tau}{\sigma_{\infty}}$), where G_{∞} is the unrelaxed elastic shear modulus (typically assumed to be a constant for silicate melts at $\sim 10^{10}\,\text{Pa}$; [8]). Combining the structural relaxation equation with the Adam-Gibbs theory of melt relaxation gives [26]:

$$\eta(T) = A_e \exp\left(\frac{B_e}{TS^{conf}(T)}\right) \tag{1}$$

where A_e is a pre-exponential term and high-temperature viscosity limit of the melt, and B_e is a constant proportional to the Gibbs free-energy barriers hindering rearrangements in the melt.

The variation of configurational entropy with temperature is defined as:

$$S^{conf}(T) = S^{conf}(T_g) + \int_{T_g}^{T} \frac{C_P^{conf}}{T} dT$$
 (2)

where C_P^{conf} is the difference in heat capacity between the melt and the glass and may be obtained by calorimetry [25,26,29] and $S^{conf}(T_g)$ is the configurational entropy of the melt at the glass transition. Although $S^{conf}(T_g)$ may only be directly obtained by calorimetry for congruently melting compositions, comprehensive calorimetry and viscosity datasets allow $S^{conf}(T_g)$ to be fitted, just like the A_e and B_e parameters, when Eqs. 1 and 2 are combined. We refer to fits obtained through configurational entropy modelling as "Adam-Gibbs" or "AG" for short. Other successful viscosity models exist (e.g., Tamman-Vogel-Fulcher, Avramov-Milchev, and MYEGA models; [3,22,43]), but the AG model is particularly interesting because it allows for the possibility of using independently measured heat capacity to predict viscosity and, as we use it in this paper, to predict thermodynamic properties of a system using viscosity data.

For viscosity, deviations from linearity upon mixing are most important at temperatures near the glass transition (T_g) and are smaller at superliquidus temperatures. At low temperatures near the glass transition, there is a greater relative contribution of configurational entropy, which includes chemical (mixing) and topological (distribution of bond angles and bond lengths) components, whereas the heat capacity of the liquid is the most important term at higher temperatures ([18,26], Eq. 2). Although some studies investigating Ca-Mg cation mixing in silicate melts have found the assumption of ideal mixing to be appropriate (e.g., [25]), this does not appear to be the case for Na-K aluminosilicate or Mg-K (alumino)silicate melts (e.g., [2,18,19]). We propose a configurational entropy model for mixed-alkali aluminosilicate melts of the (Na,K)AlSiO₄-SiO₂ system spanning Al/Si ratios between 0.2 and 1.

2. Experimental methods

2.1. Sample synthesis

We weighed reagent grade oxide (SiO₂, Al₂O₃) and carbonate (Na₂CO₃, K₂CO₃) powders using a Sartorius Cubis analytical balance. We mixed the powders under acetone for \sim 20 min. We transferred the slurry in roughly equal amounts into two separate PtRh crucibles of 120 mL capacity and known weight. Each slurry was ignited and the acetone allowed to burn off. We let the dry mixtures cool in a desiccator. After weighing, we heated the dry mixtures very slowly overnight to 1100 °C in a Nabertherm box furnace to drive off CO₂.

We fused the decarbonated powder mixtures to temperatures between 1600 and 1745 °C and immediately quenched the glass upon reaching temperature. The glass was then completely tapped out of each crucible, combined and mechanically ground with a high density alumina dish and puck in a Spex® ShatterBox® swing mill. We carefully scraped out the powdered glass out of the dish and put it into a single crucible for melting. For each melting step, we kept the melt at

Table 1Chemical and physical sample characterization.

Sample	Ne_{100}	Ne ₇₅	Ne _{62.5}	Ne_{50}	Ne _{37.5}	Ne_{25}	Jd_{100}	Jd ₇₅	$Jd_{62.5}$	Jd_{50}	$Jd_{37.5}$	Jd_{25}	Jd_0	Or	K-petalite
no. of analyses	18	17	20	16	30	17	12	11	18	10	25	5	3	6	6
(wt%)															
SiO_2	40.51	39.41	40.33	37.87	39.34	37.28	57.32	55.98	57.12	54.85	55.86	53.12	54.51	63.38	71.56
Al_2O_3	37.12	35.87	35.01	34.84	33.80	34.17	26.14	25.49	24.66	24.79	23.77	24.76	25.04	18.93	17.63
FeO	0.04	0.04	0.04	0.05	0.00	0.06	0.04	0.06	0.01	0.05	0.03	0.05	0.00	0.04	0.15
Na ₂ O	21.61	15.74	13.29	10.11	7.57	4.89	15.24	11.34	9.24	7.27	5.57	3.52	0.07	0.04	0.06
K ₂ O	0.02	8.29	12.26	16.07	19.52	22.62	0.03	5.92	8.68	11.54	14.22	17.12	21.57	15.97	15.37
Total	99.29	99.36	100.92	98.94	100.23	99.02	98.76	98.79	99.72	98.50	99.49	98.57	101.19	98.36	104.77
std (wt%)															
SiO_2	0.60	0.55	0.16	0.45	0.29	0.60	0.88	1.19	0.41	0.79	0.59	1.54	0.29	0.41	1.04
Al_2O_3	0.28	0.24	0.35	0.21	0.24	0.22	0.44	0.69	0.28	0.38	0.40	1.23	0.10	0.10	0.06
FeO	0.01	0.02	0.02	0.02	0.00	0.02	0.02	0.02	0.01	0.03	0.02	0.02	0.01	0.02	0.02
Na ₂ O	0.15	0.13	0.09	0.13	0.07	0.11	0.22	0.28	0.09	0.15	0.14	0.14	0.01	0.01	0.01
K ₂ O	0.01	0.09	0.09	0.10	0.11	0.16	0.00	0.07	0.10	0.15	0.12	0.17	0.05	0.16	0.30
mol.%															
SiO_2	48.61	48.60	49.39	48.27	49.77	48.68	65.50	65.26	66.28	65.41	66.24	64.75	65.60	74.78	77.95
Al_2O_3	26.24	26.06	25.26	26.17	25.20	26.29	17.60	17.51	16.86	17.42	16.61	17.79	17.76	13.16	11.31
Na ₂ O	25.14	18.81	15.77	12.50	9.28	6.19	16.88	12.82	10.39	8.40	6.41	4.16	0.08	0.04	0.06
K ₂ O	0.02	6.52	9.57	13.06	15.75	18.84	0.02	4.40	6.43	8.77	10.75	13.31	16.56	12.02	10.68
Total	100.00	100.00	100.00	100.00	100.00	100.00	100.00	100.00	100.00	100.00	100.00	100.00	100.00	100.00	100.00
NBO/T	-0.02	-0.01	0.00	-0.01	0.00	-0.02	-0.01	-0.01	0.00	0.00	0.01	-0.01	-0.02	-0.02	-0.01
$Al/(Al + Si)^a$	0.52	0.52	0.51	0.52	0.50	0.52	0.35	0.35	0.34	0.35	0.33	0.35	0.35	0.26	0.22
$Na/(Na + K)^a$	1.00	0.74	0.62	0.49	0.37	0.25	1.00	0.74	0.62	0.49	0.37	0.24	0.00	0.00	0.01
gfw ^b	71.55	73.58	74.22	75.73	76.19	77.64	67.78	69.16	69.51	70.53	70.83	72.15	73.17	69.69	68.46
no. of atoms	3.52	3.52	3.51	3.52	3.50	3.53	3.35	3.35	3.34	3.35	3.33	3.36	3.36	3.26	3.23
(kg/m ₃)															
ρ_{pre}^{c}	2487(2)	2489(2)	2492(2)	2487(1)	2488(1)	2481(2)	2411(2)	2412(3)	2411(2)	2409(2)	2408(2)	2396(2)	2333	2288	2333
ρ_{post}^{d}	2500(2)	2497(2)	2496(2)	2494(2)	2492(1)	2487(2)	2417(1)	2422(3)	2416(1)	2417(2)	2412(1)	2407(2)	2334	n.a.	2337
Bubble fraction	< 0.01	< 0.01	~0.18	< 0.01	< 0.05	< 0.01	< 0.05	< 0.05	< 0.05	< 0.05	< 0.05	< 0.05	< 0.01	n.d.	n.d.

All samples are nominally anhydrous and expected to contain < 0.1 wt% dissolved water [33]. This corresponds to an effect on the glass transition temperature of at most 20 K [5].

Measurements of compositions post parallel-plate and concentric cylinder viscosity experiments are provided as supplementary material. Post-experiment analyses overlap with pre-experiment analyses, within the analytical uncertainty of the order of 0.2-0.3 wt% for Na_2O or K_2O , except in the case where samples crystallized during an experiment and crystals affected the composition of the glass.

- ^a Cation units.
- ^b Gram formula weight for one mole of oxides, equivalent to a two oxygen basis in this system.
- ^c Density of glass before viscometry measurement. Standard deviation on 5 measurements in parentheses.
- ^d Density of glass after parallel-plate viscometry measurement. Standard deviation on 5 measurements in parentheses.

maximum temperature for one to two hours, and quenched it to a glass by pouring it onto a copper tray. We crushed and remelted the glass slabs two or three more times, until we obtained a homogeneous, bubble-free, and crystal-free glass. Melting temperatures varied between 1600 and 1750 $^{\circ}$ C. For some very viscous melts, we were not able to obtain entirely bubble-free glasses. The estimated bubble fraction for those glasses is in Table 1.

We drilled the glass slabs to produce 5 mm (quarter inch) diameter cylinders roughly one centimeter long. We cut parallel ends for each cylinder using a low-speed wafer saw, and polished the cylinder ends to obtain smooth parallel surfaces.

2.2. Sample characterization

We measured the composition of the glasses pre- and post-viscometry experiments with a Cameca SX-50 electron microprobe at the University of Massachusetts – Amherst (Table 1). We tried to mitigate Na migration by using a low beam current density, that is, by using a beam diameter of 20 µm and a beam current of 10 nA at an accelerating voltage of 15 kV. Counting for Na was done on a very high count rate monochromator (Cameca's PCO detector, otherwise known as the ovonyx W-Si multilayer with 2d-spacing of 60 Å), which allows short count times with good precision. This allowed us to measure Na with 6 s counting on peak to minimize any inaccuracies arising from both diffusion (migration of Na toward space charge) and surface carbon buildup. Matrix corrections are done via Cameca's PAP program which

is integrated into the quantitative analysis package within the SXRayN50 automation.

We measured the density of the glass cores before and after parallel-plate viscometry experiments (Table 1). We used the Archimedean method, with anhydrous ethanol as the immersion liquid. Each density reported is an average of five measurements. We estimated bubble or crystal fraction (in the case where samples crystallized during experiments) by transmitted light microscopy. We did not observe crystals in the starting glasses.

2.3. Viscometry

We measured the viscosity of melts at low temperatures near the glass transition by parallel-plate viscometry ($\eta=10^{8.5}$ – $10^{13}\,\mathrm{Pa}\,\mathrm{s}$) at Bates College. The instrument recovers viscosity data within 0.1 log units as tested by measuring National Institute of Standards and Technology SRM 717a glass over the full range of viscosities testable. Samples generally underwent < 10% shortening during the viscosity measurements and the cores maintained a cylindrical shape. We therefore calculated viscosity from the shortening rate of the samples at constant load using the perfect slip condition [7], using the following equation:

$$\eta_s = \frac{mgh^2}{3V\frac{dh}{dt}} \tag{3}$$

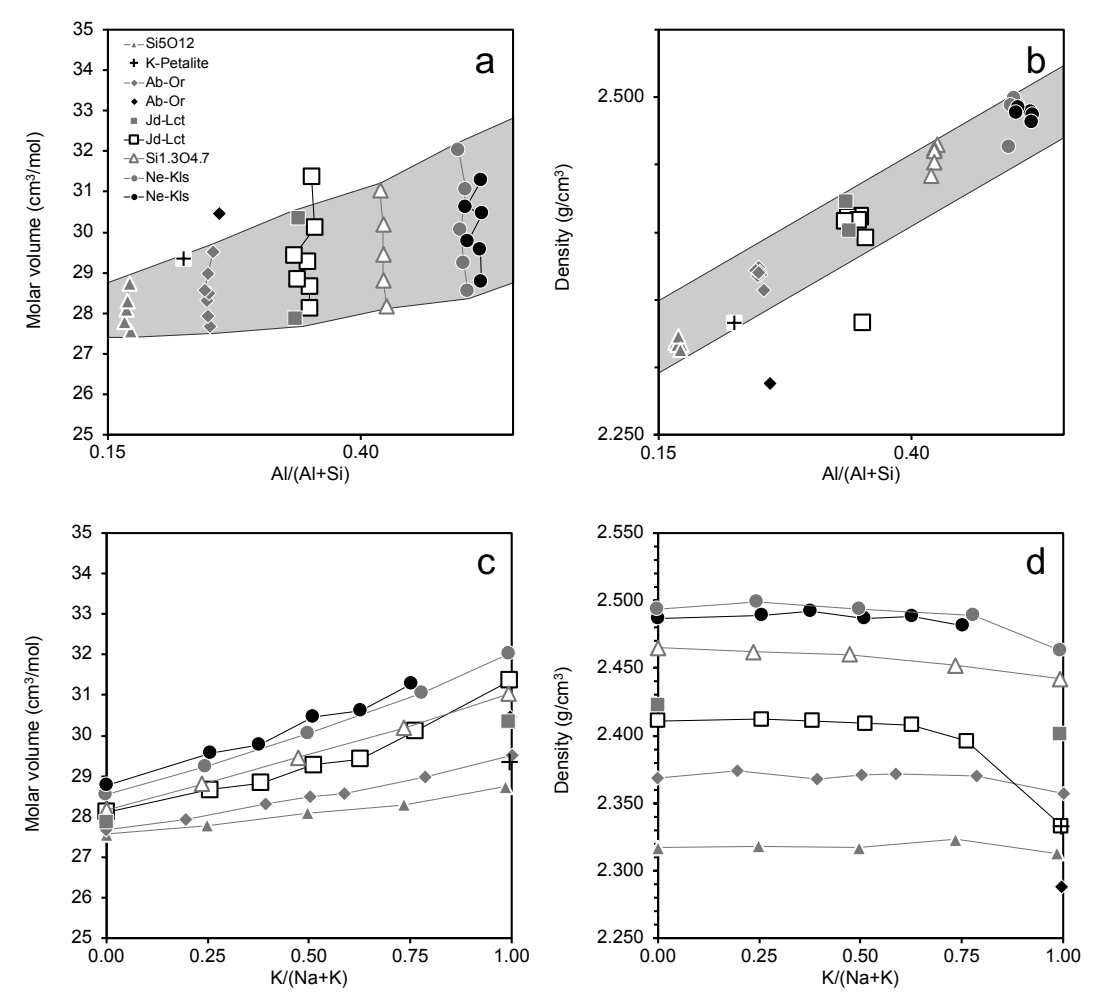


Fig. 2. Black symbols: this study. Open triangles and diamonds: Le Losq and Neuville [18]. Grey circles, grey triangles, and squares: Le Losq et al. [19]. Shaded areas highlight trends in the data.

where m is the mass applied to the sample (kg), g gravity (ms⁻²), h the sample height (m), V the volume of the sample (m³), and t is time (s). We report the viscometric glass transition as the temperature at which the viscosity is $10^{12} \, \text{Pa} \, \text{s} \, (T_{12})$.

We measured the viscosity of melts at high temperature ($\eta = 1$ to 105 Pas) in the concentric-cylinder viscometer at the University of Missouri - Columbia using a Theta Industries Rheotronic II Rotating Viscometer, equipped with a Brookfield HBDV-III Ultra measuring head and full range spring torque of 57,496·10⁻⁴ Nm). The crucible holding the melt and the cylindrical spindle rotating inside of the melt are both PtRh alloy. The instrument measures the torque exerted by the melt on the spindle rotating at a constant angular velocity, at a given temperature. For each temperature, we record the torque for three different angular velocities to test for any non-Newtonian behavior. The viscosity we report for a given temperature is an average of the viscosity calculated for each angular velocity. The instrument is calibrated using NIST standards. The liquidus temperature of the melt investigated was generally the lower temperature limit for a given experiment, except for melts that exceeded the viscosity limit of the instrument or which were surprisingly stable in the supercooled state. Ne₅₀ is the most potassiumrich composition we were able to measure using the instrument at the University of Missouri - Columbia. Melts with more potassium than Ne₅₀ have liquidus temperatures higher than the upper limit of the instrument. Similarly, we were only able to obtain 2 measurements on sample Jd_{25} because of crystallization at temperatures near the upper limit of the instrument. We sent samples of Ne_{37.5} and Ne₂₅ to Anton-Paar in Ostfildern, Germany, for measurements at higher temperature.

The samples were measured in a Anton-Paar FRS 1800, DSR 502 rheometer. Sample $Ne_{37.5}$ was measured in an Ar atmosphere using a graphite crucible and spindle, and Ne_{25} was measured in air using an alumina crucible and spindle. Measurements reported for $Ne_{37.5}$ and Ne_{25} were performed at 1750 °C. We estimate the uncertainty on viscosity to be < 0.1 log units, based on comparison with measurements on standard melts NIST 710a and 717a [10].

3. Experimental results

3.1. Density

Overall, density is relatively constant across a join up to X_K ratios of 0.5, then decreases slightly at higher X_K (Fig. 2d). Density variations across a join range from 1 to 3.5%. Density decreases linearly from highest Al/Si ratio to lowest Al/Si ratio (Fig. 2b). For any given Al/Si ratio, the increase in molar volume caused by the substitution of K for Na is roughly a linear function of the K/(Na + K) ratio; this increase is more important at higher Al/Si ratio (Fig. 2a, c). These changes reflect changes in density across a join ranging from $\sim 4 \, \text{kg/m}^3$ for high SiO₂ glasses to $\sim 30 \, \text{kg/m}^3$ for low SiO₂ glasses. There is a larger spread in molar volume for glass compositions with higher Al/Si (3.5 cm³/mol) ratio than for glass compositions with small Al/Si ratios (1.3 cm³/mol). The potassium end-members range from 28.7 to 32.0 and sodium end-members range from 27.6 to 28.8 cm³/mol.

All samples have a higher density post parallel-plate viscometry than pre-viscometry (Table 1). All synthesized samples had fewer than

Table 2 Viscosity data – *JdLct*.

	Jd_{100}				$Jd_{62.5}$				$Jd_{37.5}$				Jd_0		
T (K)	$\log \eta$ (log Pa.s)	order		T (K)	log η (log Pa.s)	order		T (K)	log η (log Pa.s)	order		T (K)	$\log \eta$ (log Pa.s)	order	
1103	11.25	6	PP	1082	11.76	8a	PP	1123	12.08	10a	PP	1195	13.02	10	I
1113	10.90	4	PP	1142	10.51	7a	PP	1148	11.36	6a	PP	1204	12.73	9	F
1122	10.71	2	PP	1161	10.16	4a	PP	1162	11.13	8a	PP	1214	12.45	8	I
1127	10.49	7	PP	1179	9.84	5a	PP	1173	10.85	9a	PP	1219	12.30	15	I
1136	10.39	3	PP	1191	9.60	3a	PP	1191	10.43	4a	PP	1224	12.28	7]
1146	10.04	5	PP	1217	9.16	11a	PP	1198	10.30	7a	PP	1229	12.07	14]
1170	9.58	1	PP	1774	3.59	3b	CC	1222	9.84	3a	PP	1234	12.02	6	I
1177	9.50	9	PP	1799	3.42	4b	CC	1230	9.72	5a	PP	1238	11.86	13	I
1710	3.61	8b	CC	1824	3.25	2b	CC	1244	9.51	11a	PP	1244	11.79	5	F
1742	3.39	7b	CC	1849	3.09	5b	CC	1819	3.61	4b	CC	1249	11.60	11	I
1763	3.25	6b	CC	1866	2.98	6b	CC	1840	3.47	3b	CC	1254	11.47	4	F
1783	3.12	5b	CC	1866	2.99	1b	CC	1854	3.37	5b	CC	1257	11.54	12	F
1803	2.99	4b	CC					1860	3.34	2b	CC	1263	11.29	10a	F
1824	2.87	3b	CC					1864	3.30	6b	CC	1266	11.24	12	F
1841	2.77	2b	CC					1869	3.28	1b	CC	1269	11.28	11	F
1854	2.68	9Ъ	CC					1870	3.26	7b	CC	1270	11.17	2	I
1864	2.64	1b	CC												
Jd ₇₅					Jd_{50}				Jd_{25}						
T (K)	$\log \eta$ (log Pa.s)	order		T (K)	log η (log Pa.s)	order		T (K)	log η (log Pa.s)	order					
1057	12.07	10b	PP	1087	12.09	10b	PP								
1072	11.80	8b	PP	1102	11.67	8b	PP	1163	11.66	6	PP				
	11.80 11.44	8b 9b	PP PP	1102 1132	11.67 11.15	8b 6b	PP PP	1163 1186	11.66 11.00	6 7	PP PP				
1088				1102 1132 1153	11.67 11.15 10.74			1163 1186 1195							
1088 1103	11.44	9Ъ	PP	1132	11.15	6b	PP	1186	11.00	7	PP				
1088 1103 1107	11.44 11.13	9b 5a	PP PP	1132 1153	11.15 10.74	6b 5a	PP PP	1186 1195	11.00 10.75	7 3	PP PP				
1072 1088 1103 1107 1113 1122	11.44 11.13 10.96	9b 5a 6b	PP PP PP	1132 1153 1156	11.15 10.74 10.62 10.34	6b 5a 7a	PP PP PP	1186 1195 1205	11.00 10.75 10.58	7 3 5	PP PP PP				
1088 1103 1107 1113	11.44 11.13 10.96 10.78	9b 5a 6b 7b	PP PP PP PP	1132 1153 1156 1166 1166	11.15 10.74 10.62	6b 5a 7a 7b	PP PP PP PP	1186 1195 1205 1227	11.00 10.75 10.58 10.04	7 3 5 1	PP PP PP PP				
1088 1103 1107 1113 1122 1134	11.44 11.13 10.96 10.78 10.70	9b 5a 6b 7b 2a 4a	PP PP PP PP PP	1132 1153 1156 1166 1166 1175	11.15 10.74 10.62 10.34 10.30 10.21	6b 5a 7a 7b 1a 6a	PP PP PP PP PP	1186 1195 1205 1227 1252 1256	11.00 10.75 10.58 10.04 9.73 9.74	7 3 5 1 9	PP PP PP PP PP				
1088 1103 1107 1113 1122 1134 1136	11.44 11.13 10.96 10.78 10.70 10.48 10.42	9b 5a 6b 7b 2a	PP PP PP PP	1132 1153 1156 1166 1166 1175 1192	11.15 10.74 10.62 10.34 10.30 10.21 9.92	6b 5a 7a 7b 1a 6a	PP PP PP PP PP PP	1186 1195 1205 1227 1252 1256 1852	11.00 10.75 10.58 10.04 9.73 9.74 3.62	7 3 5 1 9 8 2b	PP PP PP PP PP PP				
1088 1103 1107 1113 1122 1134 1136 1146	11.44 11.13 10.96 10.78 10.70 10.48	9b 5a 6b 7b 2a 4a 3a	PP PP PP PP PP	1132 1153 1156 1166 1166 1175	11.15 10.74 10.62 10.34 10.30 10.21	6b 5a 7a 7b 1a 6a	PP PP PP PP PP	1186 1195 1205 1227 1252 1256	11.00 10.75 10.58 10.04 9.73 9.74	7 3 5 1 9	PP PP PP PP PP				
1088 1103 1107 1113 1122 1134	11.44 11.13 10.96 10.78 10.70 10.48 10.42 10.18	9b 5a 6b 7b 2a 4a 3a 6a	PP PP PP PP PP PP	1132 1153 1156 1166 1166 1175 1192 1200	11.15 10.74 10.62 10.34 10.30 10.21 9.92 9.74 9.65	6b 5a 7a 7b 1a 6a 3a	PP PP PP PP PP	1186 1195 1205 1227 1252 1256 1852 1865	11.00 10.75 10.58 10.04 9.73 9.74 3.62 3.49	7 3 5 1 9 8 2b 1b	PP PP PP PP CC CC				
1088 1103 1107 1113 1122 1134 1136 1146 1151	11.44 11.13 10.96 10.78 10.70 10.48 10.42 10.18 10.01	9b 5a 6b 7b 2a 4a 3a 6a 4b	PP PP PP PP PP PP PP	1132 1153 1156 1166 1166 1175 1192 1200 1202	11.15 10.74 10.62 10.34 10.30 10.21 9.92 9.74	6b 5a 7a 7b 1a 6a 3a 4a 5b	PP PP PP PP PP PP PP	1186 1195 1205 1227 1252 1256 1852 1865	11.00 10.75 10.58 10.04 9.73 9.74 3.62 3.49	7 3 5 1 9 8 2b 1b	PP PP PP PP CC CC				
1088 1103 1107 1113 1122 1134 1136 1146 1151 1159 1163	11.44 11.13 10.96 10.78 10.70 10.48 10.42 10.18 10.01 9.85 9.79	9b 5a 6b 7b 2a 4a 3a 6a 4b 5b	PP	1132 1153 1156 1166 1166 1175 1192 1200 1202 1213 1216	11.15 10.74 10.62 10.34 10.30 10.21 9.92 9.74 9.65 9.44 9.43	6b 5a 7a 7b 1a 6a 3a 4a 5b 3b	PP	1186 1195 1205 1227 1252 1256 1852 1865	11.00 10.75 10.58 10.04 9.73 9.74 3.62 3.49	7 3 5 1 9 8 2b 1b	PP PP PP PP CC CC				
1088 1103 1107 1113 1122 1134 1136 1146 1151 1159	11.44 11.13 10.96 10.78 10.70 10.48 10.42 10.18 10.01 9.85	9b 5a 6b 7b 2a 4a 3a 6a 4b 5b	PP PP PP PP PP PP PP PP PP	1132 1153 1156 1166 1166 1175 1192 1200 1202 1213	11.15 10.74 10.62 10.34 10.30 10.21 9.92 9.74 9.65 9.44	6b 5a 7a 7b 1a 6a 3a 4a 5b	PP PP PP PP PP PP PP PP	1186 1195 1205 1227 1252 1256 1852 1865	11.00 10.75 10.58 10.04 9.73 9.74 3.62 3.49	7 3 5 1 9 8 2b 1b	PP PP PP PP CC CC				
1088 1103 1107 1113 1122 1134 1136 1146 1151 1159 1163 1186 1198	11.44 11.13 10.96 10.78 10.70 10.48 10.42 10.18 10.01 9.85 9.79 9.33 9.12	9b 5a 6b 7b 2a 4a 3a 6a 4b 5b 8a 3b 11b	PP	1132 1153 1156 1166 1166 1175 1192 1200 1202 1213 1216 1225 1240	11.15 10.74 10.62 10.34 10.30 10.21 9.92 9.74 9.65 9.44 9.43 9.30 9.02	6b 5a 7a 7b 1a 6a 3a 4a 5b 3b 2a 9a 11b	PP	1186 1195 1205 1227 1252 1256 1852 1865	11.00 10.75 10.58 10.04 9.73 9.74 3.62 3.49	7 3 5 1 9 8 2b 1b	PP PP PP PP CC CC				
1088 1103 1107 1113 1122 1134 1136 1146 1151 1159 1163 1186 1198 1745	11.44 11.13 10.96 10.78 10.70 10.48 10.42 10.18 10.01 9.85 9.79 9.33	9b 5a 6b 7b 2a 4a 3a 6a 4b 5b 8a 3b	PP	1132 1153 1156 1166 1166 1175 1192 1200 1202 1213 1216 1225	11.15 10.74 10.62 10.34 10.30 10.21 9.92 9.74 9.65 9.44 9.43 9.30	6b 5a 7a 7b 1a 6a 3a 4a 5b 3b 2a 9a	PP	1186 1195 1205 1227 1252 1256 1852 1865	11.00 10.75 10.58 10.04 9.73 9.74 3.62 3.49	7 3 5 1 9 8 2b 1b	PP PP PP PP CC CC				
1088 1103 1107 1113 1122 1134 1136 1146 1151 1159 1163 1186 1198 1745	11.44 11.13 10.96 10.78 10.70 10.48 10.42 10.18 10.01 9.85 9.79 9.33 9.12 3.55	9b 5a 6b 7b 2a 4a 3a 6a 4b 5b 8a 3b 11b 4c	PP	1132 1153 1156 1166 1166 1175 1192 1200 1202 1213 1216 1225 1240 1711	11.15 10.74 10.62 10.34 10.30 10.21 9.92 9.74 9.65 9.44 9.43 9.30 9.02 3.95	6b 5a 7a 7b 1a 6a 3a 4a 5b 3b 2a 9a 11b 10c	PP	1186 1195 1205 1227 1252 1256 1852 1865	11.00 10.75 10.58 10.04 9.73 9.74 3.62 3.49	7 3 5 1 9 8 2b 1b	PP PP PP PP CC CC				
1088 1103 1107 1113 1122 1134 1136 1146 1151 1159 1163 1186	11.44 11.13 10.96 10.78 10.70 10.48 10.42 10.18 10.01 9.85 9.79 9.33 9.12 3.55 3.38	9b 5a 6b 7b 2a 4a 3a 6a 4b 5b 8a 3b 11b 4c 3c	PP CC CC	1132 1153 1156 1166 1166 1175 1192 1200 1202 1213 1216 1225 1240 1711 1735	11.15 10.74 10.62 10.34 10.30 10.21 9.92 9.74 9.65 9.44 9.43 9.30 9.02 3.95 3.76	6b 5a 7a 7b 1a 6a 3a 4a 5b 3b 2a 9a 11b 10c 9c	PP CC CC	1186 1195 1205 1227 1252 1256 1852 1865	11.00 10.75 10.58 10.04 9.73 9.74 3.62 3.49	7 3 5 1 9 8 2b 1b	PP PP PP PP CC CC				
1088 1103 1107 1113 1122 1134 1136 1146 1151 1159 1163 1186 1198 1745 1771 1796	11.44 11.13 10.96 10.78 10.70 10.48 10.42 10.18 10.01 9.85 9.79 9.33 9.12 3.55 3.38 3.21	9b 5a 6b 7b 2a 4a 3a 6a 4b 5b 8a 3b 11b 4c 3c 5c	PP CC CC C	1132 1153 1156 1166 1166 1175 1192 1200 1202 1213 1216 1225 1240 1711 1735 1758	11.15 10.74 10.62 10.34 10.30 10.21 9.92 9.74 9.65 9.44 9.43 9.30 9.02 3.95 3.76 3.60	6b 5a 7a 7b 1a 6a 3a 4a 5b 3b 2a 9a 11b 10c 9c 8c	PP CC CC C	1186 1195 1205 1227 1252 1256 1852 1865	11.00 10.75 10.58 10.04 9.73 9.74 3.62 3.49	7 3 5 1 9 8 2b 1b	PP PP PP PP CC CC				
1088 1103 1107 1113 1122 1134 1136 1146 1151 1159 1163 1186 1198 1745 1771 1796 1822 1847	11.44 11.13 10.96 10.78 10.70 10.48 10.42 10.18 10.01 9.85 9.79 9.33 9.12 3.55 3.38 3.21 3.05 2.89	9b 5a 6b 7b 2a 4a 3a 6a 4b 5b 8a 3b 11b 4c 3c 5c 2c 6c	PP CC CC CC C	1132 1153 1156 1166 1166 1175 1192 1200 1202 1213 1216 1225 1240 1711 1735 1758 1758 1782 1807	11.15 10.74 10.62 10.34 10.30 10.21 9.92 9.74 9.65 9.44 9.43 9.30 9.02 3.95 3.76 3.60 3.44 3.26	6b 5a 7a 7b 1a 6a 3a 4a 5b 3b 2a 9a 11b 10c 9c 8c 7c	PP CC CC C	1186 1195 1205 1227 1252 1256 1852 1865	11.00 10.75 10.58 10.04 9.73 9.74 3.62 3.49	7 3 5 1 9 8 2b 1b	PP PP PP PP CC CC				
1088 1103 1107 1113 1122 1134 1136 1146 1151 1159 1163 1186 1198 1745 1771 1796 1822 1847 1864	11.44 11.13 10.96 10.78 10.70 10.48 10.42 10.18 10.01 9.85 9.79 9.33 9.12 3.55 3.38 3.21 3.05 2.89 2.80	9b 5a 6b 7b 2a 4a 3a 6a 4b 5b 8a 3b 11b 4c 3c 5c 2c	PP CC CC CC C	1132 1153 1156 1166 1166 1175 1192 1200 1202 1213 1216 1225 1240 1711 1735 1758 1782 1807 1826	11.15 10.74 10.62 10.34 10.30 10.21 9.92 9.74 9.65 9.44 9.43 9.30 9.02 3.95 3.76 3.60 3.44	6b 5a 7a 7b 1a 6a 3a 4a 5b 3b 2a 9a 11b 10c 9c 8c 7c 6c	PP CC CC C	1186 1195 1205 1227 1252 1256 1852 1865	11.00 10.75 10.58 10.04 9.73 9.74 3.62 3.49	7 3 5 1 9 8 2b 1b	PP PP PP PP CC CC				
1088 1103 1107 1113 1122 1134 1136 1146 1151 1159 1163 1186 1198 1745 1771 1796 1822 1847	11.44 11.13 10.96 10.78 10.70 10.48 10.42 10.18 10.01 9.85 9.79 9.33 9.12 3.55 3.38 3.21 3.05 2.89	9b 5a 6b 7b 2a 4a 3a 6a 4b 5b 8a 3b 11b 4c 3c 5c 2c 6c 1c	PP CC CC CC C	1132 1153 1156 1166 1166 1175 1192 1200 1202 1213 1216 1225 1240 1711 1735 1758 1758 1782 1807	11.15 10.74 10.62 10.34 10.30 10.21 9.92 9.74 9.65 9.44 9.43 9.30 9.02 3.95 3.76 3.60 3.44 3.26 3.16	6b 5a 7a 7b 1a 6a 3a 4a 5b 3b 2a 9a 11b 10c 9c 8c 7c 6c 11c	PP CC CC CC C	1186 1195 1205 1227 1252 1256 1852 1865	11.00 10.75 10.58 10.04 9.73 9.74 3.62 3.49	7 3 5 1 9 8 2b 1b	PP PP PP PP CC CC				

PP: Parallel-plate viscometry.

Order: Order in which viscosity measurements were performed. Order resets for each viscometry method and is indicated by a letter following the number. If multiple viscosity experiments were performed using one method on a given sample, this is also indicated by a letter following the number.

5% bubbles, except for $Ne_{62.5}$, which had between 15 and 20%. We expect bubbles to have little effect on viscosity measurements. Density measurements for samples in each of the two joins are in good agreement with those of Le Losq and Neuville [18] and Le Losq et al. [19], except for our leucite and orthoclase samples, which have densities ~4% lower (Fig. 2). We used the density model of Lange [17] to recalculate density and molar volume at $T=1098\,\mathrm{K}$ for compositions along each join. When the density data are normalized to the same fictive temperature, we see a slight increase $(1-3\,\mathrm{kg/m^3})$ in density with increasing K along the Si_5O_{12} and AbOr joins. For all other joins, a decrease in density is observed with increasing K, and this decrease becomes more important at higher Al/Si ratios (e.g., $3\,\mathrm{kg/m^3}$ for JdLct and $19\,\mathrm{kg/m^3}$ for NeKls). Normalizing the data to the same fictive temperature for all samples results in very good agreement between our data and those of Le Losq and Neuville [18] and Le Losq et al. [19]. The

trends in molar volume remain relatively unchanged with the normalization to a common fictive temperature, except for the molar volume of leucite decreasing from 31.36 to $30.60 \, \mathrm{cm}^3/\mathrm{mol}$, in better agreement with the data of Le Losq et al. [19]. Molar volume increases linearly with increasing K/(Na + K) along each join.

3.2. Viscosity

Viscosity data are reported in Tables 2-4. At high temperatures $(T>1300\,^{\circ}\text{C})$, jadeite-leucite (JdLct) melts have viscosities ~ 1.25 log units higher than nepheline-kalsilite (NeKls) melts (Fig. 3). For both joins, melt viscosity increases progressively with increasing potassium. Melts in both joins have approximately the same slope in the high temperature range.

At low temperatures above the glass transition (T < 1000 °C), JdLct

CC: Concentric-cylinder viscometry.

Table 3 Viscosity data – *NeKls*.

	Ne ₁₀₀				Ne _{62.5}				Ne _{37.5}		
T (K)	log η (log Pa.s)	Order		T (K)	Log η (log Pa.s)	Order		T (K)	Log η (log Pa.s)	Order	
1073	12.07	9a	PP	1087	11.80	10a	PP	1147	11.49	9	PF
1101	11.04	7b	PP	1092	11.60	8a	PP	1158	11.17	10	PF
1115	10.79	8c	PP	1107	11.22	6a	PP	1172	10.90	7	PF
1129	10.24	5	PP	1110	11.03	9a	PP	1178	10.55	8	PF
1143	9.95	6	PP	1118	10.82	7a	PP	1192	10.33	5	PI
1158	9.50	4	PP	1136	10.37	4a	PP	1211	9.82	4	PI
1811	1.70	3b	CC	1150	10.02	5a	PP	1219	9.70	6	PI
1821	1.65	5b	CC	1178	9.32	3a	PP	1238	9.29	12	PI
1830	1.60	2b	CC	1188	9.14	11a	PP	2023	1.04	1a	C
1846	1.53	1b	CC	1775	2.48	3b	CC				
1861	1.45	4b	CC	1800	2.32	4b	CC				
				1825	2.16	2b	CC				
				1851	2.01	5b	CC				
				1865	1.94	1b	CC				
				1866	1.91	6b	CC				
Ne ₇₅				Ne ₅₀				Ne_{25}			
T (K)	log η (log Pa.s)	order		T (K)	log η (log Pa.s)	order		T (K)	log η (log Pa.s)	order	
1072	11.82	10c	PP	1113	11.72	11a	PP	1183	11.49	8	PF
1078	11.89	11a	PP	1122	11.44	9a	PP	1197	10.90	6	PI
1086	11.48	8c	PP	1133	11.08	10a	PP	1220	10.50	9	Pl
1093	11.40	9a	PP	1143	10.88	7a	PP	1234	10.13	7	Pl
1100	11.24	11c	PP	1153	10.58	8a	PP	1245	9.83	1	Pl
1110	10.84	7a	PP	1163	10.32	5a	PP	1248	9.72	4	P
1114	10.66	6c	PP	1170	10.05	1a	PP	1251	9.68	3	P
1120	10.58	10a	PP	1182	9.86	3a	PP	1252	9.74	10	P
1127	10.45	7c	PP	1189	9.66	2a	PP	1264	9.43	2	P
1131	10.23	9c	PP	1198	9.51	4a	PP	1264	9.37	5	P
1135	10.20	8a	PP	1205	9.32	6a	PP	2023	0.93	1a	C
1141	10.07	12c	PP	1218	9.04	12a	PP				
1149	9.74	5a	PP	1806	2.36	3b	CC				
1152	9.66	1a	PP	1830	2.21	2b	CC				
1154	9.65	5c	PP	1840	2.15	1b	CC				
1160	9.50	6a	PP	1850	2.06	4b	CC				
1166	9.35	3a	PP								
1171	9.25	2a	PP								
1175	9.25	12a	PP								
1179	9.03	4a	PP								
1682	2.75	7b	CC								
1707	2.58	6b	CC								
1730	2.43	5b	CC								
1757	2.27	4b	CC								
1780	2.13	3b	CC								
1805	1.99	2b	CC								

PP: Parallel-plate viscometry.

CC: Concentric-cylinder viscometry.

Order: Order in which viscosity measurements were performed. Order resets for each viscometry method and is indicated by a letter following the number. If multiple viscosity experiments were performed using one method on a given sample, this is also indicated by a letter following the number.

melts have slightly higher viscosities than *NeKls* melts overall, and the rate of change in viscosity with temperature near the glass transition is higher for *NeKls* than for *JdLct* melts (Fig. 3). Orthoclase and K-petalite have shallower slopes than jadeite-leucite melts. Our viscosity measurements are in good agreement with those of Le Losq et al. [19] for nepheline-kalsilite melts, except for the sodium end-member. Our viscosity data for nepheline are also in good agreement with the measurements by Toplis et al. [40,41], but our jadeite data are \sim 0.3 log units higher, with a parallel slope.

The differences in viscosity between the melts we measured in this study are on the order of \sim 2.5 log units across the whole temperature range. For the jadeite-leucite join, there is 3.1 log units of viscosity difference between the Na- and K-end members at 1300 K; at 1823 K, the difference is 1.6 log units (Fig. 4b). Increasing K only has a small effect on T_{12} at low and intermediate K/(Na + K) ratios up to 0.4, but results in a rapid increase at higher K content (Figs. 4a and 5). Although

we did not measure the viscosity of kalsilite melt, extrapolation from available data suggests that the effects on T_{12} of substituting K for Na are similar for both joins.

Minima in isothermal viscosity occur at the sodium end-member for each join (Fig. 4b). In the low-temperature range ($T=1300\,\mathrm{K}$), viscosity varies non-linearly across a join and the mixed-alkali effect results in a depression in viscosity at intermediate Na/K ratios of as much as one log unit relative to a linear variation. In the high-temperature range ($T=1823\,\mathrm{K}$), viscosity increases with increasing K across a join is nearly linear (\pm 0.25 log units) for most joins with the exception of the JdLct join for which a viscosity depression of \sim 0.4 log units is observed at intermediate Na/K ratios. There is a difference of \sim 50 K in the temperature at which the viscosity is $10^{12}\,\mathrm{Pa.s}$ (T_{12}) between the Si_5O_{12} and the NeKls joins (Fig. 4a), with melts of higher Al/(Al + Si) ratio having the lowest T_{12} on average. At $T=1300\,\mathrm{K}$, Na-rich melts vary in viscosity from $10^{6.4}$ – $10^{8.9}\,\mathrm{Pa.s}$ across Al/Si ratios from 0.2 to 1. K-rich

Table 4 Viscosity data for *Or* and K-petalite.

K-petal	ite			Or	Or						
T (K)	log η (log Pa.s)	order		T (K)	log η (log Pa.s)	order					
1189	12.45	5	PP	1201	12.31	8	PP				
1199	12.31	8	PP	1205	12.26	23	PP				
1214	12.02	9	PP	1211	12.11	6	PP				
1223	11.93	8b	PP	1214	12.07	22	PP				
1229	11.73	7	PP	1215	12.02	15	PP				
1244	11.47	10	PP	1225	11.82	16	PP				
1252	11.33	6	PP	1226	11.77	5a	PP				
1254	11.25	4	PP	1228	11.77	5b	PP				
1262	11.13	4b	PP	1231	11.65	4	PP				
1265	11.02	2	PP	1233	11.67	6b	PP				
1268	11.07	7b	PP	1234	11.62	6a	PP				
1269	11.04	11	PP	1235	11.63	21	PP				
1274	11.03	9b	PP	1235	11.62	17	PP				
1274	10.92	6b	PP	1236	11.59	5	PP				
1279	10.86	5b	PP	1243	11.45	4	PP				
1287	10.67	3	PP	1244	11.38	7	PP				
1289	10.67	3b	PP	1245	11.44	18	PP				
				1252	11.25	7	PP				
				1252	11.24	9b	PP				
				1252	11.26	9a	PP				
				1255	11.26	19	PP				

PP: Parallel-plate viscometry.

CC: Concentric-cylinder viscometry.

Order: Order in which viscosity measurements were performed. Order resets for each viscometry method and is indicated by a letter following the number. If multiple viscosity experiments were performed using one method on a given sample, this is also indicated by a letter following the number.

melts span viscosities of $10^{9.4}$ – $10^{10.9}$ Pa.s for the same Al/Si ratios.

The data show that, overall, melts with high Al/(Al + Si) ratio are more fragile than melts with lower ratios (Fig. 4d). This is also seen in the slopes of the viscosity data near the glass transition in Fig. 3. T_{12} varies in a different way as a function of Al/(Al + Si) ratio for Na and K end-member melts (Fig. 5a). The largest difference of temperature at the glass transition (T_{12}) between the end-member melts happens at an Al/(Al + Si) ratio of ~ 0.35 –0.43, that is, for the *JdLct* and $Si_{1.3}O_{4.7}$ joins. This is both because of the higher viscosities of the K end-member and because these joins have lower viscosities for their Na end-members relative to the melts on other Al/(Al + Si) ratio joins. The largest ΔT_{12} occurs at the $Si_{1.3}O_{4.7}$ join (Fig. 5b).

4. Modelling

4.1. Tamman-Vogel-Fulcher empirical fits

We report empirical fits to the viscosity data for each of the samples studied in Table 5. We fitted the viscosity data using three approaches: i) fit each sample individually without imposing constraints on any of the parameters, ii) fit each sample individually constraining $A_{TVF} = -4.3$ as per Russell et al. [32], and iii) impose a common, but unconstrained A_{TVF} to all samples along the same join. In Figs. 4e and f, we compare the fit parameters obtained with the constraint of A = -4.3 for our samples and those of Le Losq and Neuville [18] and Le Losq et al. [19]. B_{TVF} shows an overall increase with increasing X_K , except for our NeKls measurements which increase until $X_K = 0.4$ and then decrease at higher X_K . C_{TVF} shows a concave up trend across the joins, with lowest values at intermediate X_K . Fragility (Eq. 4) decreases slightly overall with increasing X_K , except for our NeKls measurements

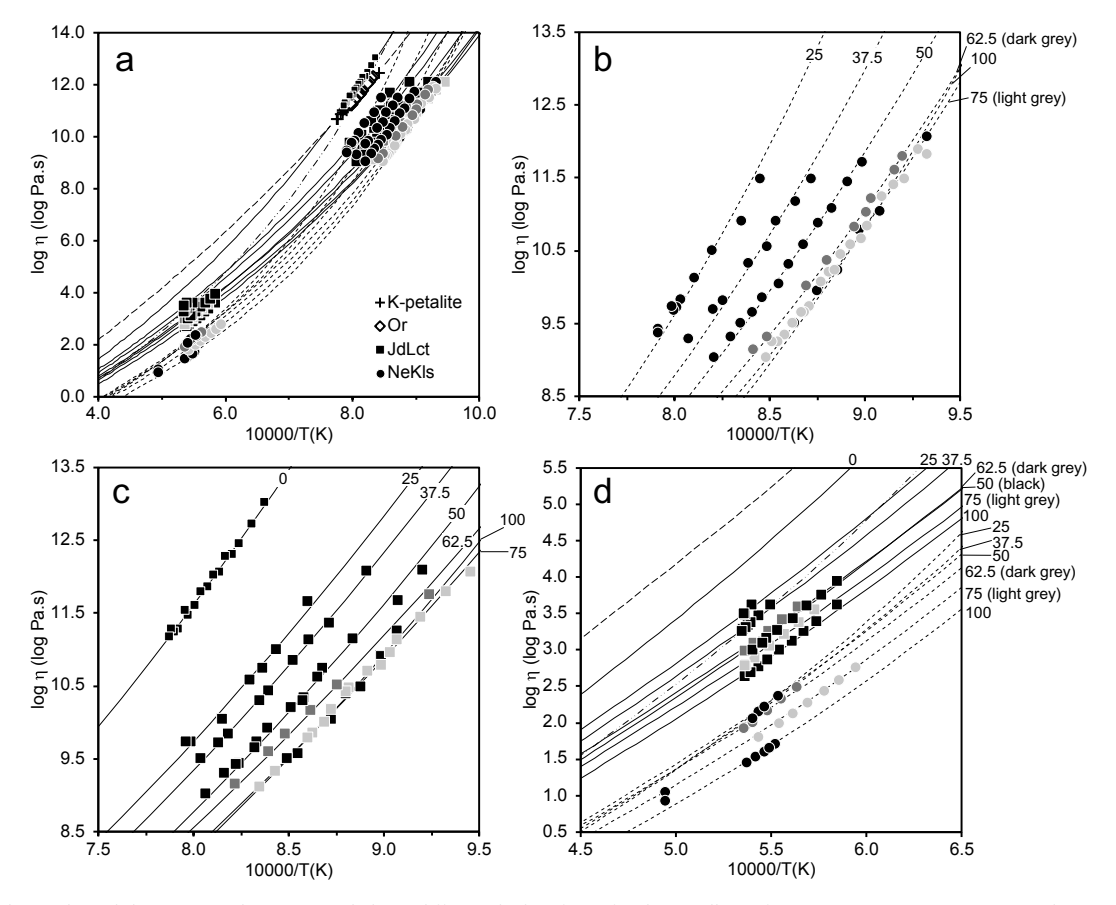


Fig. 3. All symbols as in legend shown in panel a. Some symbols are different shades of grey for clarity. All TVF fits use a constant A parameter equal to -4.3 [32]. Numbers next to TVF fits refer to sodium end-member content (e.g., "25" on a dashed line means Ne_{25}). a. Viscosity data for all melts measured in this study, over the full temperature range. b. Near-glass transition viscosity data for nepheline-kalsilite melts. c. Near-glass transition viscosity data for jadeite-leucite melts. d. High-temperature range.

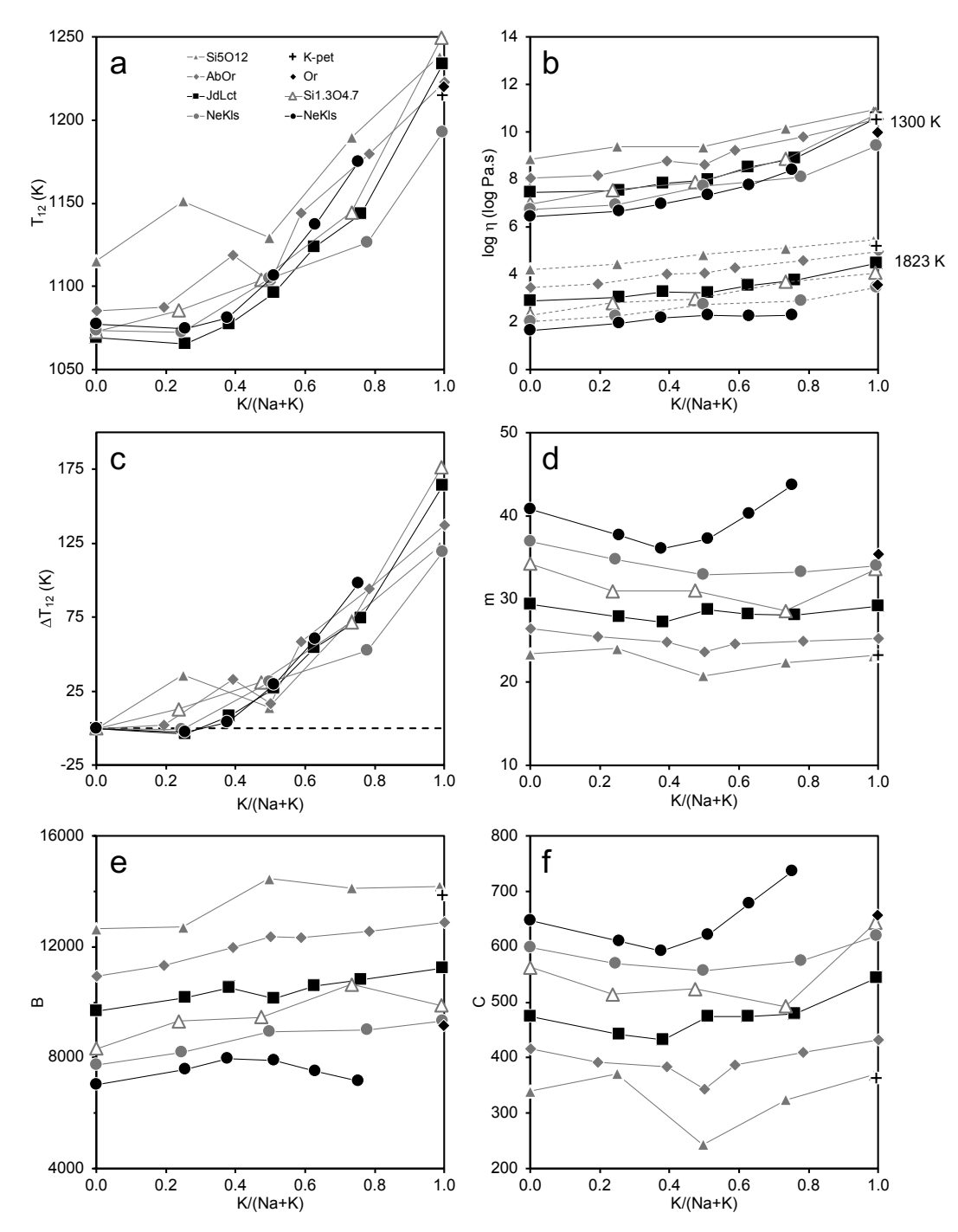


Fig. 4. a. T_{12} vs. X_K . b. Isotherms for T=1300 K (high viscosity) and T=1823 K (low viscosity). Lines are dashed for extrapolated data. c. ΔT_{12} (relative to sodium end-member) vs. X_K . d. Fragility (m) as calculated by Eq. 4 vs. X_K . e and f: TVF fit parameters. All data reported using a constant A parameter equal to -4.3 [32]. All symbols as in legend shown in panel a.

and the $Si_{1.3}O_{4.7}$ join which show a minimum at intermediate X_K (Fig. 4d).

$$m = \frac{B_{TVF}}{T_{12} \left(1 - \frac{c_{TVF}}{T_{12}}\right)^2} \tag{4}$$

Root-mean-square deviation (RMSD) values obtained by TVF fitting are slightly better when A^{TVF} is unconstrained for an individual composition or is a common, but unconstrained value for a given join (Table 5). The greatest improvement of fit is for the *NeKls* join. When A is unconstrained, it varies between -5.8 and -5.0 for *NeKls*, JdLct, and Or, and returns a value of -11.4 for K-petalite.

4.2. Configurational entropy modelling

4.2.1. Individual compositions

We used configurational entropy modelling to obtain values of A_e , B_e , and $S^{conf}(T_g)$ (Eqs. 1 and 2). We used the model of Richet [27] for the heat capacity of multicomponent oxide glass. This model predicts a smooth, and very small, decrease for the heat capacity of the glass at the glass transition temperature as X_K increases. We used the model of Stebbins et al. [35] for the heat capacity of the liquid. This model predicts trends parallel to those of the glass, when calculated at the glass transition temperature, but we note that the model does not account for temperature-dependent liquid heat capacity (e.g., [4,28]).

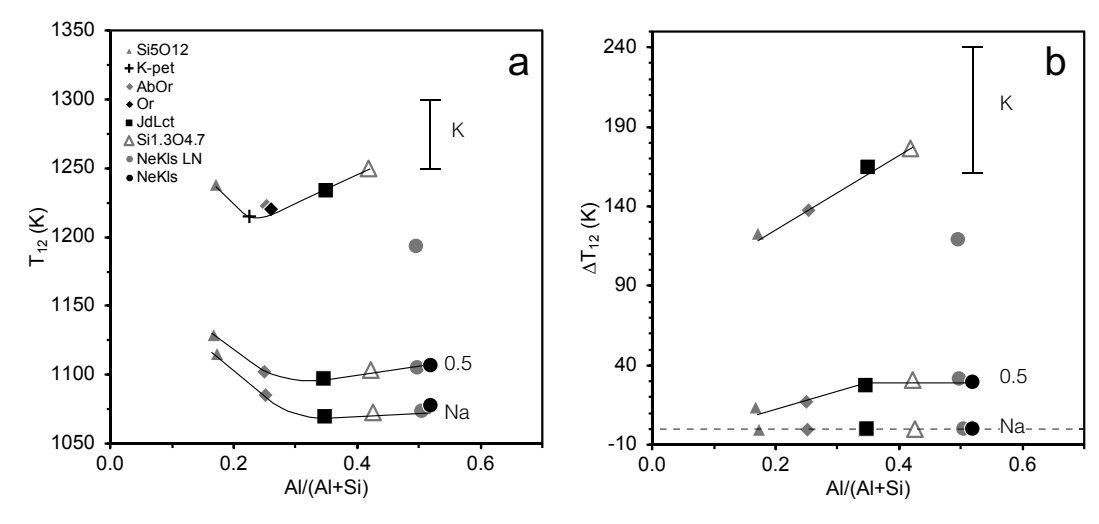


Fig. 5. a. T_{12} vs. X_{Al} , and b. ΔT_{12} (relative to sodium end-member) vs. X_{Al} . All symbols as in legend shown in panel a. Vertical bars at Al/(Al + Si) = 0.52 represent extrapolations of our viscosity data ($T_{12} \sim 1300$ K and $\Delta T_{12} \sim 200$ K) to the K end-member for the NeKls join, which predict much higher values than those of Le Losq et al. [19]. Values for the Na end-members, K end-members, and for K/(Na + K) = 0.5 are shown.

Table 5 TVF parameters for fits to individual compositions following equation: $\log(\eta) = A + \frac{B}{I-C}$.

Sample	n	\mathbf{A}_{ind}^{TVF}	\mathbf{B}_{ind}^{TVF}	C_{ind}^{TVF}	RMSD	T ₁₂ (K)	т
K-petalite	17	-4.30	13,878	363.3	0.04	1215	23.3
Or	21	-4.30	12,446	452.7	0.02	1216	26.0
Jd_{100}	17	-4.30	9687	475.0	0.05	1069	29.3
Jd_{75}	22	-4.30	10,157	442.1	0.05	1065	27.9
$Jd_{62.5}$	12	-4.30	10,523	431.9	0.05	1077	27.2
Jd_{50}	24	-4.30	10,141	474.3	0.07	1096	28.7
$Jd_{37.5}$	16	-4.30	10,584	474.5	0.03	1124	28.2
Jd_{25}	10	-4.30	10,816	479.8	0.07	1143	28.1
Jd_0	16	-4.30	11,241	543.8	0.04	1233	29.2
JdLct ^a	117				0.06		
Ne ₁₀₀	11	-4.30	7016	646.9	0.07	1077	40.8
Ne ₇₅	27	-4.30	7578	609.6	0.08	1075	37.7
Ne _{62.5}	15	-4.30	7978	591.7	0.04	1081	36.0
Ne ₅₀	16	-4.30	7905	621.6	0.06	1107	37.2
Ne _{37.5}	9	-4.30	7501	677.2	0.15	1137	40.3
Ne ₂₅	11	-4.30	7150	736.3	0.17	1175	43.7
NeKls ^a	89				0.10		
Sample		Λ TVF	D TVF	C TVF	DATED	T (II)	
Janiple	n	\mathbf{A}_{join}^{TVF}	\mathbf{B}_{join}^{TVF}	C_{join}^{TVF}	RMSD	T ₁₂ (K)	m
K-petalite ^b	17	-11.37	28,412	0.0	0.04	1 ₁₂ (K)	23.4
K-petalite ^b	17	-11.37	28,412	0.0	0.04	1216	23.4
K-petalite ^b Or ^b	17	-11.37 -5.80	28,412 14,882	0.0 380.2	0.04 0.02	1216 1216	23.4 25.9
K-petalite ^b Or ^b Jd ₁₀₀	17	-11.37 -5.80 -5.01	28,412 14,882 11,136	0.0 380.2 411.6	0.04 0.02 0.06	1216 1216 1066	23.4 25.9 27.7
K-petalite ^b Or ^b Jd ₁₀₀ Jd ₇₅	17	-11.37 -5.80 -5.01 -5.01	28,412 14,882 11,136 11,613	0.0 380.2 411.6 380.3	0.04 0.02 0.06 0.05	1216 1216 1066 1063	23.4 25.9 27.7 26.5
K-petalite ^b Or ^b Jd ₁₀₀ Jd ₇₅ Jd _{62.5}	17	-11.37 -5.80 -5.01 -5.01 -5.01	28,412 14,882 11,136 11,613 12,042	0.0 380.2 411.6 380.3 366.5	0.04 0.02 0.06 0.05 0.03	1216 1216 1066 1063 1074	23.4 25.9 27.7 26.5 25.8
K-petaliteb Orb $Jd100$ $Jd75$ $Jd62.5$ $Jd50$	17	-11.37 -5.80 -5.01 -5.01 -5.01 -5.01	28,412 14,882 11,136 11,613 12,042 11,563	0.0 380.2 411.6 380.3 366.5 414.1	0.04 0.02 0.06 0.05 0.03 0.05	1216 1216 1066 1063 1074 1094	23.4 25.9 27.7 26.5 25.8 27.4
K-petalite ^b Or ^b Jd ₁₀₀ Jd ₇₅ Jd _{62.5} Jd ₅₀ Jd _{37.5}	17	-11.37 -5.80 -5.01 -5.01 -5.01 -5.01 -5.01	28,412 14,882 11,136 11,613 12,042 11,563 12,087	0.0 380.2 411.6 380.3 366.5 414.1 411.1	0.04 0.02 0.06 0.05 0.03 0.05 0.04	1216 1216 1066 1063 1074 1094 1122	23.4 25.9 27.7 26.5 25.8 27.4 26.9
K-petalite ^b Or ^b Jd ₁₀₀ Jd ₇₅ Jd _{62.5} Jd ₅₀ Jd _{37.5} Jd ₂₅	17	-11.37 -5.80 -5.01 -5.01 -5.01 -5.01 -5.01	28,412 14,882 11,136 11,613 12,042 11,563 12,087 12,334	0.0 380.2 411.6 380.3 366.5 414.1 411.1 415.7	0.04 0.02 0.06 0.05 0.03 0.05 0.04 0.08	1216 1216 1066 1063 1074 1094 1122 1141	23.4 25.9 27.7 26.5 25.8 27.4 26.9 26.8
K-petalite ^b Or ^b Jd ₁₀₀ Jd ₇₅ Jd _{62.5} Jd ₅₀ Jd _{37.5} Jd ₂₅ Jd ₀	17 21	-11.37 -5.80 -5.01 -5.01 -5.01 -5.01 -5.01	28,412 14,882 11,136 11,613 12,042 11,563 12,087 12,334	0.0 380.2 411.6 380.3 366.5 414.1 411.1 415.7	0.04 0.02 0.06 0.05 0.03 0.05 0.04 0.08	1216 1216 1066 1063 1074 1094 1122 1141	23.4 25.9 27.7 26.5 25.8 27.4 26.9 26.8
K-petalite ^b Or ^b Jd ₁₀₀ Jd ₇₅ Jd _{62.5} Jd ₅₀ Jd _{37.5} Jd ₂₅ Jd ₀ JdLct ^a	17 21	-11.37 -5.80 -5.01 -5.01 -5.01 -5.01 -5.01 -5.01 -5.01	28,412 14,882 11,136 11,613 12,042 11,563 12,087 12,334 12,244	0.0 380.2 411.6 380.3 366.5 414.1 411.1 415.7 513.7	0.04 0.02 0.06 0.05 0.03 0.05 0.04 0.08 0.04	1216 1216 1066 1063 1074 1094 1122 1141 1233	23.4 25.9 27.7 26.5 25.8 27.4 26.9 26.8 29.2
K-petalite ^b Or ^b Jd ₁₀₀ Jd ₇₅ Jd _{62.5} Jd ₅₀ Jd _{37.5} Jd ₂₅ Jd ₀ JdLct ^a Ne ₁₀₀	17 21	-11.37 -5.80 -5.01 -5.01 -5.01 -5.01 -5.01 -5.01 -5.01	28,412 14,882 11,136 11,613 12,042 11,563 12,087 12,334 12,244	0.0 380.2 411.6 380.3 366.5 414.1 411.1 415.7 513.7	0.04 0.02 0.06 0.05 0.03 0.05 0.04 0.08 0.04 0.05 0.04	1216 1216 1066 1063 1074 1094 1122 1141 1233	23.4 25.9 27.7 26.5 25.8 27.4 26.9 26.8 29.2
K-petalite ^b Or ^b Jd ₁₀₀ Jd ₇₅ Jd _{62.5} Jd ₅₀ Jd _{37.5} Jd ₂₅ Jd ₀ JdLct ^a Ne ₁₀₀ Ne ₇₅	17 21	-11.37 -5.80 -5.01 -5.01 -5.01 -5.01 -5.01 -5.01 -5.01 -5.63 -5.63	28,412 14,882 11,136 11,613 12,042 11,563 12,087 12,334 12,244 9290 9795	0.0 380.2 411.6 380.3 366.5 414.1 411.1 415.7 513.7 546.2 514.7	0.04 0.02 0.06 0.05 0.03 0.05 0.04 0.08 0.04 0.05 0.04	1216 1216 1066 1063 1074 1094 1122 1141 1233	23.4 25.9 27.7 26.5 25.8 27.4 26.9 26.8 29.2
K-petalite ^b Or ^b Jd ₁₀₀ Jd ₇₅ Jd _{62.5} Jd ₅₀ Jd _{37.5} Jd ₂₅ Jd ₀ JdLct ^a Ne ₁₀₀ Ne ₇₅ Ne _{62.5}	17 21	-11.37 -5.80 -5.01 -5.01 -5.01 -5.01 -5.01 -5.01 -5.63 -5.63 -5.63	28,412 14,882 11,136 11,613 12,042 11,563 12,087 12,334 12,244 9290 9795 10,413	0.0 380.2 411.6 380.3 366.5 414.1 411.1 415.7 513.7 546.2 514.7 486.4	0.04 0.02 0.06 0.05 0.03 0.05 0.04 0.08 0.04 0.05 0.04 0.06 0.05	1216 1216 1066 1063 1074 1094 1122 1141 1233 1069 1066 1073	23.4 25.9 27.7 26.5 25.8 27.4 26.9 26.8 29.2 32.1 30.9 29.1 30.3 31.3
K-petalite ^b Or ^b Jd ₁₀₀ Jd ₇₅ Jd _{62.5} Jd ₅₀ Jd _{37.5} Jd ₂₅ Jd ₀ JdLct ^a Ne ₁₀₀ Ne ₇₅ Ne _{62.5} Ne ₅₀	17 21	-11.37 -5.80 -5.01 -5.01 -5.01 -5.01 -5.01 -5.01 -5.63 -5.63 -5.63	28,412 14,882 11,136 11,613 12,042 11,563 12,087 12,334 12,244 9290 9795 10,413 10,246	0.0 380.2 411.6 380.3 366.5 414.1 411.1 415.7 513.7 546.2 514.7 486.4 520.7	0.04 0.02 0.06 0.05 0.03 0.05 0.04 0.08 0.04 0.05 0.04 0.05 0.04	1216 1216 1066 1063 1074 1094 1122 1141 1233 1069 1066 1073 1097	23.4 25.9 27.7 26.5 25.8 27.4 26.9 26.8 29.2 32.1 30.9 29.1 30.3

Values either fit with the constraint A=-4.3 (top) or with common A for each join (bottom).

The patterns are the same for both the *NeKls* and *JdLct* joins. We used the viscometric glass transition (T_{12}) as calculated with TVF fits with constraint A=-4.3 as T_g in the modelling. We show results obtained

by fitting each sample individually without any constraints on the Adam-Gibbs parameters, and we provide data from the literature for comparison in Table 6 and Fig. 6. The individual configurational entropy model fits all return equivalent RMSD values as for individual, unconstrained TVF fits, or better RMSD values than TVF fits when A^{TVF} is constrained to -4.3 (Table 5). The only exception to this is KAlSi₃O₈, which is better fit by TVF. Overall, the values we obtain for parameters A_e , B_e , and $S^{conf}(T_g)$ are reasonable, but there is significant noise. The JdLct join shows an obvious peak in B_e and $S^{conf}(T_g)$ at intermediate K/(Na + K) ratios (Fig. 6). Our fits show a greater range of values across the NeKls and AbOr joins than those presented by Le Losq et al. [19] who constrained the A_e parameter for each join. Our unconstrained results suggest a dependence of the fit parameters on Al/Si ratio, whereas there is no systematic variation with respect to Na/K ratio.

4.2.2. Parameterization of the (Na,K)AlSiO₄-SiO₂ system

We also used the models for the heat capacity of the glass [27] and that of the liquids [35] to investigate all viscosity datasets for which multiple compositions across a join of constant Al/Si ratio were available within the (Na,K)AlSiO₄-SiO₂ system. The A_e parameter was either treated as having a common, but unconstrained value for all compositions along each join of constant Al/Si ratio, or as being -3.51 [31]. We used forms allowing for non-ideal mixing for both the B_e and the $S^{conf}(T_g)$ parameters.

 B_e is the enthalpy term:

$$B_e = X_{Na}B_{Na} + (1 - X_{Na})B_K + w_B X_{Na}(1 - X_{Na})$$
(5)

where B_{Na} is the value of B_e for the sodium end-member, B_K is the value of B_e for the potassium end-member, X_{Na} is the mole fraction of sodium across a join, and w_B is the Margules parameter for B_e . The first two terms of Eq. 5 represent linear (ideal) symmetrical mixing and the third term is a non-ideal mixing term that reduces to ideal mixing when $w_B = 0$

 $S^{conf}(T_g)$ is the entropy term:

$$S^{conf}(T_g) = X_{Na} S^{conf}(T_g)_{Na} + (1 - X_{Na}) S^{conf}(T_g)_K$$

$$-R[X_{Na} ln X_{Na} + (1 - X_{Na}) ln (1 - X_{Na})]$$

$$+ w_S X_{Na} (1 - X_{Na})$$
(6)

where $S^{conf}(T_g)_{Na}$ is the value of $S^{conf}(T_g)$ for the sodium end-member, $S^{conf}(T_g)_K$ is the value of $S^{conf}(T_g)$ for the potassium end-member, X_{Na} is the mole fraction of sodium across a join, R is the gas constant, and w_S is the Margules parameter for $S^{conf}(T_g)$. The first three terms of Eq. 6 represent ideal mixing and the third term is a non-ideal mixing term with

^a Overall RMSD values for the whole join.

 $^{^{\}rm b}$ Values for individual composition with A = unconstrained.

a symmetrical form across the join. We tested an asymmetrical form but did not obtain better fits. All fit parameters obtained for $A_e = -3.51$ and B_e and the $S^{conf}(T_g)$ as in Eqs. 5 and 6 above are shown in Fig. 7.

RMSD values for the joins range from 0.11 to 0.23. Parameters B_{Na} , B_K , w_b , $S^{conf}(T_g)_{Na}$, and $S^{conf}(T_g)_K$ show a negative linear relationship with Al/Si ratio. Overall, B_K is smaller than B_{Na} , and $S^{conf}(T_g)_K$ is smaller than $S^{conf}(T_g)_{Na}$. We see a larger difference between the Na and K end members of the B_e and $S^{conf}(T_g)$ parameters at lower Al/Si ratio. Parameter w_s has a much weaker relationship with Al/Si ratio.

4.2.3. Global fit

We expanded our modelling of the viscosity of melts in the $(Na,K)AlSiO_4$ -SiO₂ system to also include compositions along the endmember joins SiO_2 -NaAlSiO₄ and SiO_2 -KAlSiO₄ [24,30,37,40–42] in addition to our data and those of Le Losq and Neuville [18] and Le Losq et al. [19]. A total of 49 datasets were included, representing 598 viscosity data points. None of these studies reported measurements of

dissolved water contents for their samples and we consider them nominally anhydrous and all similarly affected by any dissolved water (< 0.1 wt., [5,33]). Our high-temperature viscosity data for nepheline melt agree with those of Toplis et al. [41] and Riebling [30]. The nepheline data of N'dala et al. [24] are roughly one log unit higher viscosity for the same temperatures. At temperatures near the glass transition, there is good agreement between our data and Toplis et al. [41] and Le Losq et al. [19]. Our high-temperature viscosity data for jadeite are about 0.3 log units higher than previous data [30,37,41]. This is also the case at temperatures near the glass transition, when compared to the data of Toplis et al. [41].

Based on our parameterization results shown in Fig. 7, we chose to use the non-ideal symmetrical mixing forms for parameters B_e and $S^{conf}(T_g)$ and parameterize the end-member values and Margules parameters as a function of X_{Al} , as follows:

$$B_{Na} = b_{Na}^1 + b_{Na}^2 X_{Al} (7)$$

Table 6Configurational entropy modelling unconstrained fit results to individual compositions.

Suite	$\frac{Al}{Al + Si}$	$\frac{K}{Na+K}$	A_e^{ind}	10^{-3} B _e ^{ind}	$S^{conf}(T_g)_{ind}$	$\frac{10^{-3}B_e}{S^{conf}(T_g)}^{ind}$	RMSD	RMSI
			(log Pa s)	(KJ mol ⁻¹)	$(J mol^{-1} K^{-1})$	(10^3K)	Individual	Join
Si ₅ O ₁₂	0.17	0.00	-0.63	154.3	10.9	14.1	0.03	
Si ₅ O ₁₂	0.17	0.25	3.51	44.5	4.5	9.8	0.03	
Si ₅ O ₁₂	0.17	0.50	4.91	32.2	4.0	8.1	0.03	
Si ₅ O ₁₂	0.17	0.73	3.21	59.7	5.7	10.5	0.02	
Si ₅ O ₁₂	0.17	0.99	5.86	27.5	3.6	7.6	0.02	0.03
Na-petalite T97	0.18	0.00	-4.43	4372.0	249.7	17.5	0.06	
K-petalite	0.22	0.99	-0.34	175.3	11.7	15.0	0.04	
Ab T97	0.25	0.00	-5.72	5451.0	289.1	18.9	0.01	
Ab SS93	0.27	0.00	1.34	207.2	6.9	29.9	0.09	
AbOr	0.25	0.00	-0.08	111.6	8.5	13.1	0.09	
AbOr	0.25	0.00	-0.08 -1.27	165.5	8.5 11.5	14.4	0.01	
AbOr	0.25	0.39	-0.39	140.8	10.1	13.9	0.02	
AbOr	0.25	0.50	0.63	117.1	9.3	12.6	0.03	
AbOr	0.25	0.59	-0.75	163.5	11.2	14.6	0.04	
AbOr	0.25	0.79	0.78	111.9	8.5	13.2	0.02	
AbOr	0.25	1.00	1.56	96.8	7.6	12.8	0.03	0.02
Or	0.26	1.00	-4.51	245.5	12.2	20.1	0.08	
Jd SS93	0.32	0.00	-3.19	1486.9	91.9	16.2	0.08	
Jd SS93	0.34	0.00	-6.17	4241.2	225.8	18.8	0.05	
Jd T97	0.33	0.00	-4.38	2519.6	148.3	17.0	0.04	
JdLct	0.35	0.00	-2.64	178.9	11.4	15.7	0.05	
JdLct	0.35	0.26	-3.39	273.8	16.7	16.3	0.05	
JdLct	0.34	0.38	-4.28	417.2	24.0	17.4	0.02	
JdLct	0.35	0.51	-4.37	378.3	21.2	17.8	0.04	
JdLct	0.33	0.63	-2.87	227.2	13.6	16.7	0.03	
JdLct	0.35	0.76	-2.59	216.2	12.9	16.7	0.07	
JdLct	0.35	1.00	-2.98	237.5	12.9	18.5	0.04	0.05
60:50 T97	0.40	0.00	-4.27	2099.9	124.9	16.8	0.03	
Si _{1.4} O _{4.7}	0.43	0.00	-0.29	88.0	6.7	13.2	0.01	
Si _{1.4} O _{4.7}	0.42	0.24	-0.10	101.2	7.7	13.2	0.02	
Si _{1.4} O _{4.7}	0.42	0.47	-0.82	124.4	8.8	14.2	0.02	
Si _{1.4} O _{4.7}	0.42	0.73	1.33	88.5	7.2	12.2	0.02	
	0.42	0.73	4.24	35.9	3.7	9.7	0.02	0.02
Si _{1.4} O _{4.7} Ne T97	0.42	0.99	-3.57		68.8	16.8	0.03	0.02
Ne 197 NeKls	0.51	0.00	- 3.57 - 3.84	1156.4	10.1	16.8	0.04	
				170.9				
NeKls	0.52	0.26	-3.68	189.8	11.3	16.7	0.06	
NeKls	0.51	0.38	-3.34	185.8	11.2	16.5	0.03	
NeKls	0.52	0.51	-3.78	210.6	12.1	17.3	0.03	
NeKls	0.50	0.63	-5.01	275.3	14.4	19.1	0.05	
NeKls	0.52	0.75	-5.82	314.2	15.3	20.5	0.06	0.05
NeKls LN	0.51	0.00	1.43	55.1	4.8	11.4	0.02	
NeKls LN	0.52	0.26	-0.99	110.1	7.9	13.9	0.01	
NeKls LN	0.50	0.50	0.27	93.2	7.2	13.0	0.01	
NeKls LN	0.50	0.78	-0.24	110.1	8.0	13.8	0.03	
NeKls LN	0.50	0.99	3.03	51.4	4.8	10.7	0.02	0.02
RMSD ALL								0.04

We refit all previously published viscosity data, Si_5O_{12} , AbOr, $Si_{1.4}O_{4.7}$, NeKls LN, SS93: Ab and Jd, T97: Na-petalite, Ab, Jd, 60:50, and Ne [18,19,37,40,41].

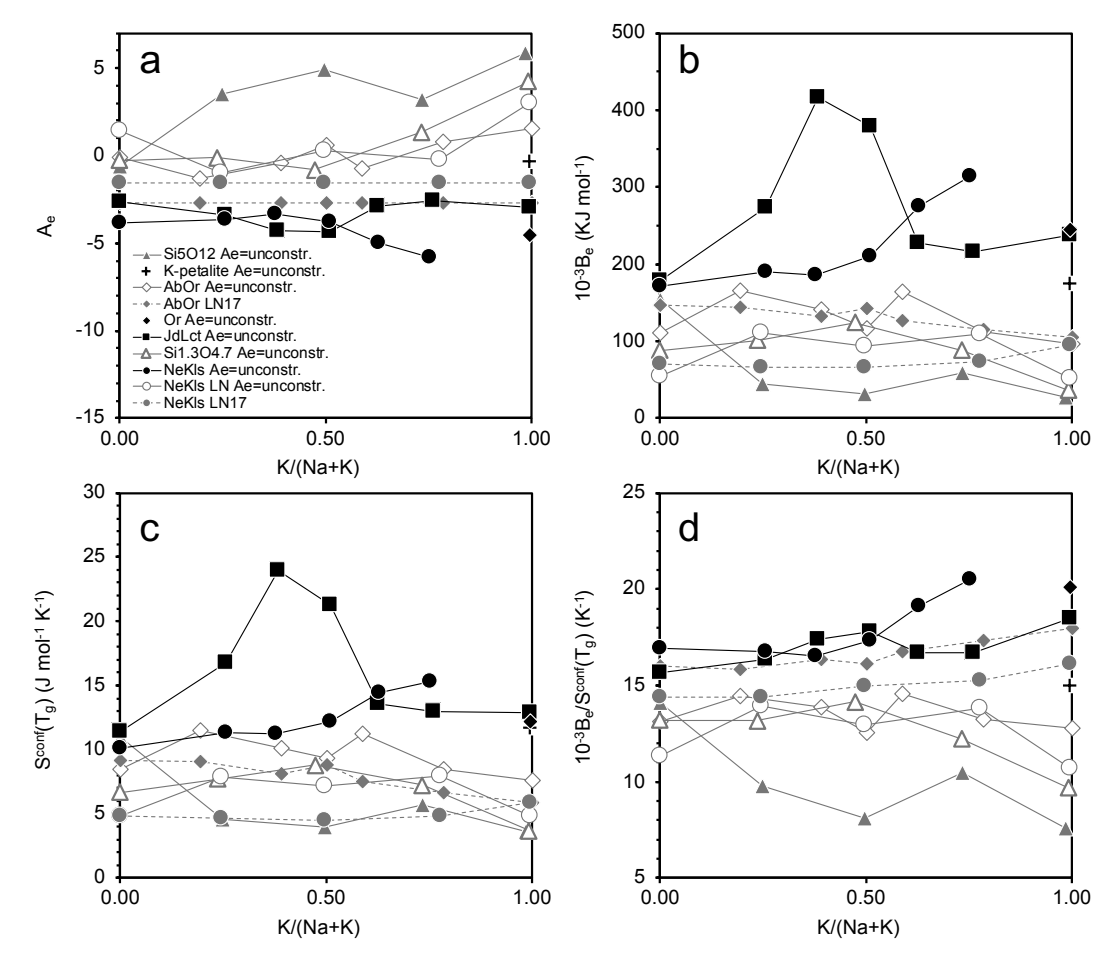


Fig. 6. Individual Adam-Gibbs fits for melts along joins in the (Na,K)AlSiO₄-SiO₂ system using model heat capacity for glass and liquid. Values for NeKls LN and AbOr LN are from Le Losq et al. [19] and have common, but unconstrained A_e value for each join instead of individual unconstrained A_e values for each composition along the join. Panels a, b, c and d show A_e , $10^{-3}B_e$, $S^{conf}(T_g)$, and $10^{-3}B_e$, $S^{conf}(T_g)$ as a function of X_K , respectively.

$$B_K = b_K^1 + b_K^2 X_{Al} (8)$$

$$w_B = w_B^1 + w_B^2 X_{Al} (9)$$

$$S^{conf}(T_g)_{Na} = c_{Na}^1 + c_{Na}^2 X_{Al}$$
 (10)

$$S^{conf}(T_g)_K = c_K^1 + c_K^2 X_{Al}$$
 (11)

$$w_S = w_S \tag{12}$$

We present two different parameterizations for A_e :

$$A_e^{-3.51} = -3.51 \tag{13}$$

$$A_e^{AlSi} = a_1 + a_2 X_{Al} \tag{14}$$

The second one (Eq. 14) allows A_e to vary as a function of Al/Si ratio as suggested by the results shown in Fig. 6a. Eqs. 5–14 break down for pure SiO₂, and we therefore exclude it from the model. Indeed, the addition of trace amounts of Al, Na, or K to SiO₂ melt dramatically changes its properties, in a non-linear way (e.g., [16,44], and references therein), whereas our model forces a linear relationship with respect to X_{Al} . Fig. 8 shows the comparison of measured vs. calculated viscosity for all of the datasets included in the model, as well as viscosity vs. reciprocal temperature fits using the model for *NeKls*, *JdLct*, *Or*, and K-Petalite compositions. Figs. 9 and 10 show the two different forms of the model. We obtain a RMSD of 0.32 for $A_e^{-3.51}$ and a RMSD of 0.26 for A_e^{AlSi} (Table 7). When A_e is constrained to a single value, we obtain a range of values between joins for the B_e and S^{conf} (T_g) parameters (Fig. 10b,c). Both parameters converge at $X_K = 1$ whereas they show a greater range in values at the sodium end-member. When A_e is allowed

to vary linearly as a function of Al/Si ratio, the $S^{conf}(T_g)$ parameter does not vary across joins (Fig. 9c). B_e^{AlSi} converges at the sodium endmember but shows a range of values at $X_K=1$ (Fig. 9b). A_e^{AlSi} varies between -2.5 and -4 (Fig. 9a). The $B_e/S^{conf}(T_g)$ ratios show similar patterns for both models, but opposite relationships with respect to Al/Si ratio (Figs. 9d and 10d).

5. Discussion

Our density data are consistent with the structural data and interpretations of Le Losq and Neuville [18] and Le Losq et al. [19] that the dilation of rings and cages in the network and the formation of percolation channels at high K in high Al/Si melts causes a significant increase of molar volume.

We note that the Kls_{99} melt of Le Losq et al. [19] has a much lower viscosity at the glass transition than what our viscosity data would predict by extrapolating our NeKls T_{12} trend to the end-member Kls. Considering that the glass structure data obtained by Raman spectroscopy and molecular dynamics simulations clearly demonstrate that the addition of K has greater effects at higher Al/(Al + Si) ratios, producing percolation channels and other changes in the melt which Le Losq and Neuville [18] and Le Losq et al. [19] have linked to the observed increase in viscosity as K/(Na + K) increases, we would not expect endmember Kls to have the lowest viscosity of all K end-member melts. If we used the extrapolation of our NeKls viscosity data instead (vertical bars in Figs. 5a,b) the magnitude of change in T_{12} relative to the Na end-member melt across a join would increase with increasing Al/(Al + Si) ratio. The viscosity data by Le Losq and Neuville [18] and Le

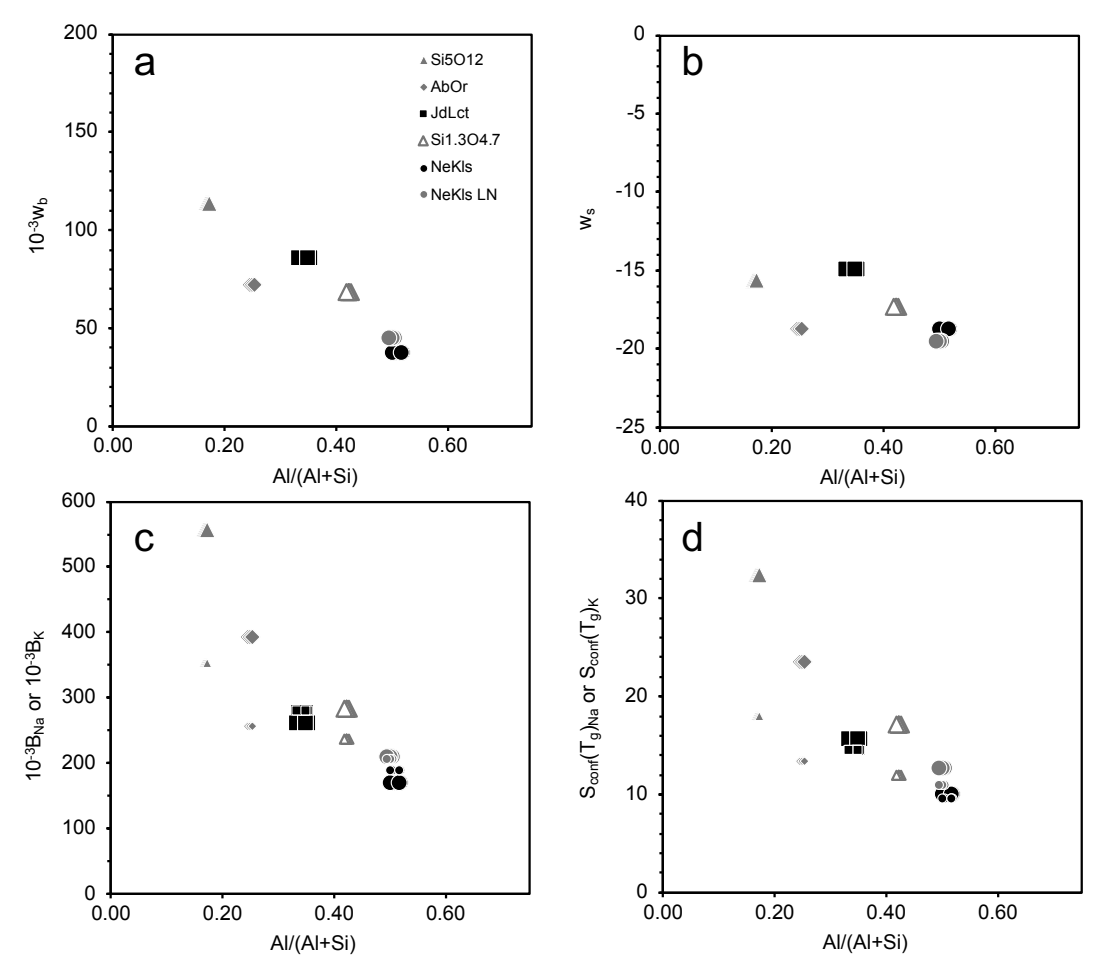


Fig. 7. Parameterization of the $(Na,K)AlSiO_4$ system. All data were obtained using model heat capacity data for glasses and liquids and fitting each join separately with Eqs. 5 and 6, and modelling A_e as a constant equal to -3.51 [31]. In panels c and d, the larger symbols are for the sodium end-member, and the smaller symbols are for the potassium end-member. There are multiple data points for a given join due to slight Al/Si ratio variations.

Losq et al. [19] instead suggest that the greatest effect on viscosity due to K/(Na + K) increase happens at intermediate Al/(Al + Si) ratios.

5.1. Configurational entropy modelling

5.1.1. Unconstrained fits to individual compositions

The goodness of fit obtained with configurational entropy modelling (AG) for individual compositions is equivalent to that of TVF (Tables 5 and 6). The overall RMSD obtained by fitting all compositions along the *JdLct* and *NeKls* joins using individual, unconstrained TVF or AG fits is ~0.05, an uncertainty equivalent or better than viscosity measurement uncertainty.

5.1.2. Global model

Fit parameters for both parameterizations of the global model are provided in Table 7, and the corresponding values of A_e , B_e , and $S^{conf}(T_g)$ are provided in Appendix Table A1. We used the same 598 data in each parameterization of the global model. Only 20 compositions have both high and low-temperature viscosity data available: 12 compositions from this study, 5 from Toplis et al. [40], and 3 from Stein and Spera [37]. Much more data are available at low temperatures near the glass transition, without any high-temperature constraints (25 datasets). Four compositions were only measured at high viscosity.

Several factors affect the goodness of fit of the global models. For example, Toplis et al. [40,41] clearly showed the effects on viscosity of small variations in composition in nominally fully-polymerized melts. Some of the older datasets do not include chemical characterization of

the samples ([24,42]), and we included them assuming the nominal compositions provided by the authors. Of the 45 analyzed compositions, 21 fall between $0.98 < (Na + K)/Al < 1.02 (<math>\pm 2\%$), and 37 between 0.95 and 1.05 (\pm 5%). All compositions that are outside of $(Na + K)/Al = 1 \pm 5\%$ are peraluminous. The largest difference is 16% relative for composition 83.8.0 from Le Losq and Neuville [18] $(Si_5O_{12} \text{ join})$, which corresponds to 0.1 log units or less variation in viscosity at 1596 °C, but to \sim 1 log unit near the glass transition [40,41]. Overall, 7 compositions are peralkaline, all within ± 5% of the metaluminous join, corresponding to a variation in viscosity of ~0.02 log units at 1596 °C and < 1 log unit near the glass transition ([40,41]). These include all compositions from Stein and Spera [37], T97 60:50 [40], $Jd_{37.5}$, $Ne_{62.5}$, and LN Ne_{75} [19]. We chose to include each dataset without any corrections, even in cases of disagreement between datasets (see Section 4.2.3) since we do not have any evidence of systematic errors in the datasets, nor can we accurately correct all compositions that are not exactly metaluminous. All of these factors, of course, introduce uncertainty in the model and it is difficult to evaluate its magnitude. However, our primary goal was to use the power of a large dataset in order to extract thermodynamic information concealed in the noise of the smaller datasets.

Our model with A_e parameterized as a function of Al/Si ratio is visibly more accurate overall than when A_e is modelled as a constant (Fig. 8). Russell and Giordano [31] obtained a A_e value of -3.51 ± 0.25 by fitting mostly complex multicomponent natural melts covering a wide range of silica contents. For binary and ternary silicate and aluminosilicate melts including nominally fully

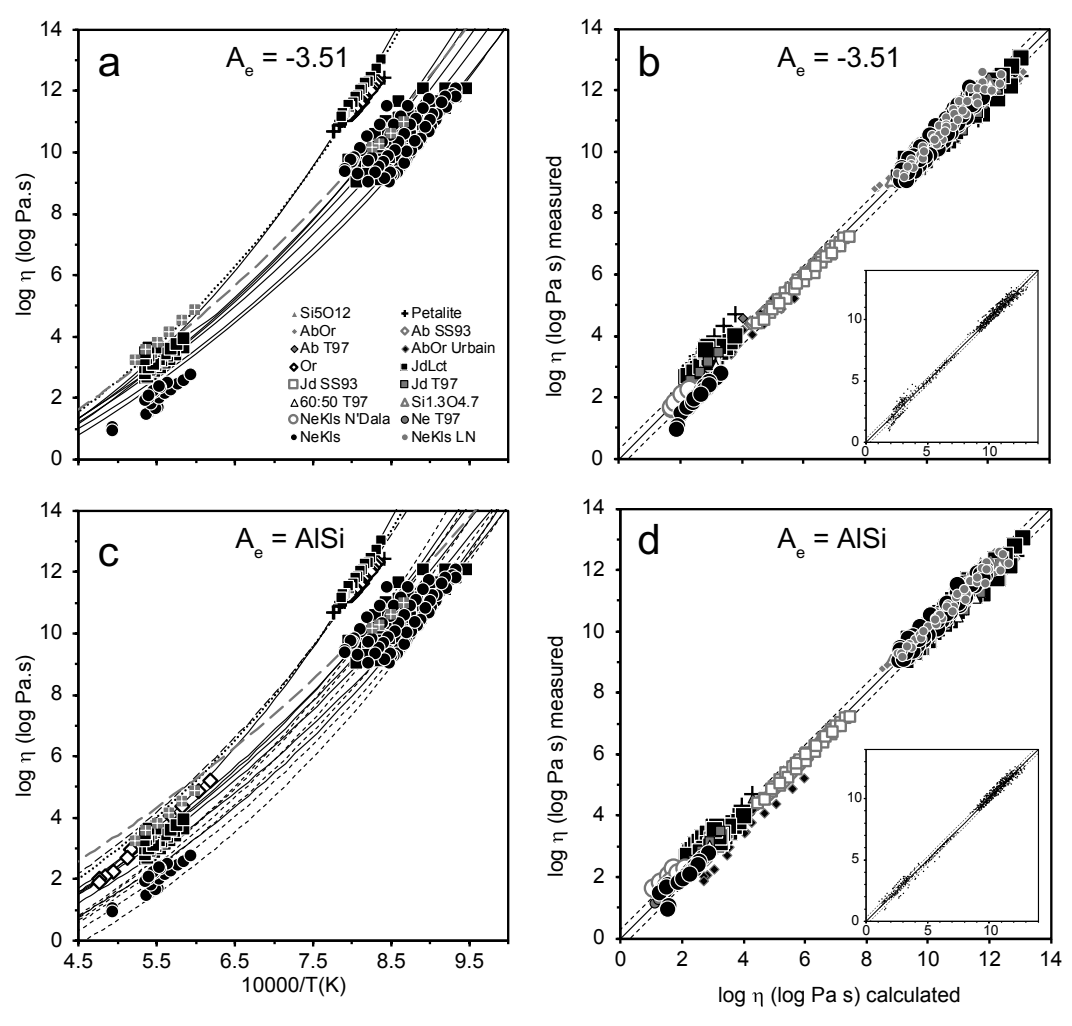


Fig. 8. Comparison of measured and calculated viscosity for the two parameterizations of the configurational entropy models: Panels a and b: $A_e = -3.51$ [31]; Panels c and d: $A_e =$ linear function of Al/Si ratio. Dashed lines in panels b and d indicate uncertainties on viscosity of \pm 0.3 log units. Symbol size has been reduced in the insets for a better visualization of the fits. Thick grey dashed line and grey symbols in panels a and c represent fits for haplogranite HPG8 [13], which was not used in the calibration of the models.

polymerized albite, jadeite, and nepheline, Toplis [39] estimated a value of -2.6 ± 1 that varied linearly as a function of $B_e/(\mathrm{Si} + \mathrm{Al})$. We obtain A_e that varies between -2.4 (Al/Si = 0.17) and -4.0 (Al/Si = 1) when we parameterize it as a function of Al/(Al + Si) ratio.

5.2. Configurational entropy at the glass transition; $S^{conf}(T_g)$

 $S^{conf}(T_g)$ varies in a concave down pattern as a function of Na/K ratio. This pattern is consistent with a positive contribution of mixing to the configurational entropy. The entropy of mixing is lower than predicted by ideal mixing (see thin solid lines in Figs. 9c and 10c), which represents a random distribution of Na and K cations in the network. When it is allowed to vary as a function of Al/Si ratio, A_e accommodates most of the variability, and $S^{conf}(T_g)$ values do not vary substantially between joins (Fig. 9c) and are closer to ideal mixing. Configurational entropy at the glass transition at $X_K = 1$ is smaller than at $X_K = 0$ for all joins and for both parameterizations of A_e (Table A1). When we hold A_e constant at -3.51, most of the variability in the model is accommodated in $S^{conf}(T_g)$ and melts of higher Al/Si ratio have the highest values. We see a spread in $S^{conf}(T_g)$ values at $X_K = 0$, and convergence for all joins at $X_K = 1$.

We recalculated $S^{conf}(T_g)$ on the basis of a gram-atom mole (Fig. 11) for a direct comparison between the different joins. For A_e^{AlSi} , patterns remain unchanged. For $A_e^{-3.51}$, there is a significant change in the

pattern where $S^{conf}(T_g)$ is highest for NeKls and lowest for Si_5O_{12} from $X_K=0$ –0.75, then the trend reverses. In both parameterizations, the values of $S^{conf}(T_g)$ are still the lowest at the potassium end-member. Patterns for isothermal configurational entropy are the same as at the glass transition for both parameterizations of A_e (Fig. 12). As expected, $S^{conf}(T=1800K)$ is higher and shows a slightly greater spread in values across all joins than $S^{conf}(T=1300K)$. All isotherms are concave down, consistent with a positive entropy of mixing and $S^{conf}(T)$ of the potassium end-member is lower than all other compositions along each join.

The similar variation in $S^{conf}(T_g)$ across a join (Fig. 11) and the small differences in $S^{conf}(T_g)$ between the different joins imply that Si-Al mixing contributes little to $S^{conf}(T_g)$, and that most of the configurational entropy at the glass transition is a result of Na-K mixing. For A_e^{AlSi} , the NeKls join has the smallest entropy of mixing for all K/ (Na + K) ratios. This could be explained by a highly ordered melt caused by the higher ratio of alkalies to network-formers, especially with the formation of percolation channels with increasing potassium as described by Le Losq et al. [19]. For $A_e^{-3.51}$, the NeKls join has the greatest entropy of mixing up to K/(Na + K) ratios of 0.7. This could be explained by greater Na-K mixing as this join has a greater ratio of alkalies to network-formers, assuming a negligible contribution of Si-Al mixing. $S^{conf}(T_g)$ of the potassium end-member melts seems unaffected by Al/Si ratio and both parameterizations predict very similar values.

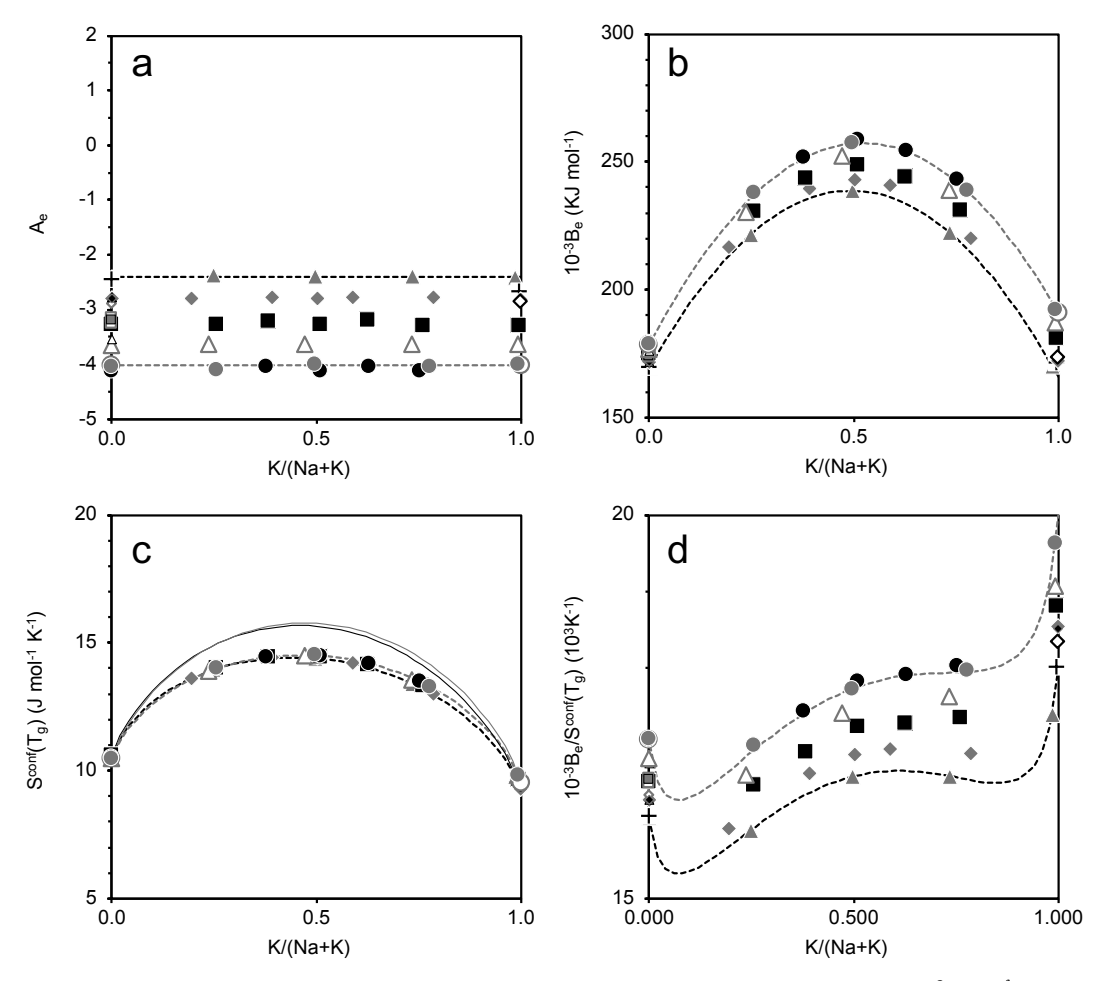


Fig. 9. Global viscosity model for system (Na,K)AlSiO₄, for A_e a linear function of Al/Si ratio. Panels a, b, c, and d show A_e , $10^{-3}B_e$, $S^{conf}(T_g)$, and $10^{-3}B_e/S^{conf}(T_g)$ as a function of X_K , respectively. Black dashed line shows model fo $X_{Al} = 0.17$, grey dashed line for $X_{Al} = 0.5$. Comparison with $S^{conf}(T_g)$ values calculated for ideal mixing is shown in panel c (thin solid lines). See Fig. 10 for legend.

Si-Al mixing therefore does not seem to provide an additional source of available configurations for the melt at high K content. Both parameterizations of A_e reproduce the viscosity data well, suggesting that chemical mixing is more important than structural changes in viscosity modelling.

The A_e^{AlSi} parameterization reproduces relationships between endmember values of $S^{conf}(T_g)$ when compared to values of residual entropy (S_0) measured independently by calorimetry [26]. Indeed, these measurements show that S_0 (reported in J g-atom⁻¹ K⁻¹) for nepheline (1.38 ± 0.30) is lower than S_0 values for both albite (2.82 ± 0.46) and orthoclase (2.18 ± 0.46) .

Le Losq et al. [19] obtained a concave down $S^{conf}(T_g)$ pattern for AbOr in which configurational entropy decreases with increasing X_K and a concave up pattern for NeKls, in which configurational entropy increases with increasing X_K . For each fit, they constrained the value of the sodium end-member to values obtained by calorimetric measurements [26]. The concave up pattern they obtain for the NeKls join is reflective of a negative configurational entropy of mixing, which would imply mixed Na-K melts have fewer available configurations relative to the end-member melts. This is not reasonable considering the mixing of Na-K results in a viscosity reduction for all joins in the (Na,K)AlSiO₄-SiO₂ systems. In addition, the increasing configurational entropy at the glass transition from the Na to the K end-member melts in NeKls calculated by Le Losq et al. [19] is inconsistent with an increase in viscosity across the join. In both parameterizations of our model, the smallest $S^{conf}(T_g)$ occurs at the potassium end-member, consistent with the higher measured viscosities.

5.3. B_e , $B_e/S^{conf}(T_e)$, and fragility

The B_e parameter follows the same patterns as $S^{conf}(T_g)$ (Figs. 9b and 10b). Values for B_e are very similar for both parameterizations of A_e , with the main difference being that $B_e^{-3.51}$ shows no spread at the potassium end-member whereas B_e^{AlSi} shows an increase with increasing Al/Si ratio.

The ratio $B_e/S^{conf}(T_g)$ is proportional to the height of the average potential energy barrier to viscous flow [39]. In both parameterizations, the average potential energy barrier to viscous flow increases with increasing potassium. However, because $S_{-3.51}^{conf}(T_g)$ shows a greater spread across Al/Si ratios, the trends as a function of Al/Si ratio for $B_e/S^{conf}(T_g)$ go in opposite directions: $B_e^{-3.51}/S_{-3.51}^{conf}(T_g)$ decreases with increasing Al/Si ratio (Fig. 10d), whereas $B_e^{AlSi}/S_{AlSi}^{conf}(T_g)$ increases (Fig. 9d). It follows that, if A_e is assumed to be constant, the *NeKls* join has the lowest potential energy barrier to viscous flow, whereas the same join has the greatest potential energy barrier to viscous flow if A_e is a linear function of Al/Si ratio. The patterns we obtain are similar in shape to those obtained by Neuville and Richet [25] for Ca-Mg mixing in pyroxene and garnet melts (shown in Fig. 5 of [39]). Values for Ab, Jd, and Ne and are within 2–3 KJ mol $^{-1}$ of the values obtained by Toplis et al. [40].

We calculated the fragility (*m*) of the melts modelled in the (Na,K)AlSiO₄ system following Toplis et al. [40]:

$$m = \frac{B_e}{T_{12}S_{conf}(T_g)} \left[1 + \frac{C_P^{conf}(T_g)}{S_{conf}(T_g)} \right]$$
 (15)

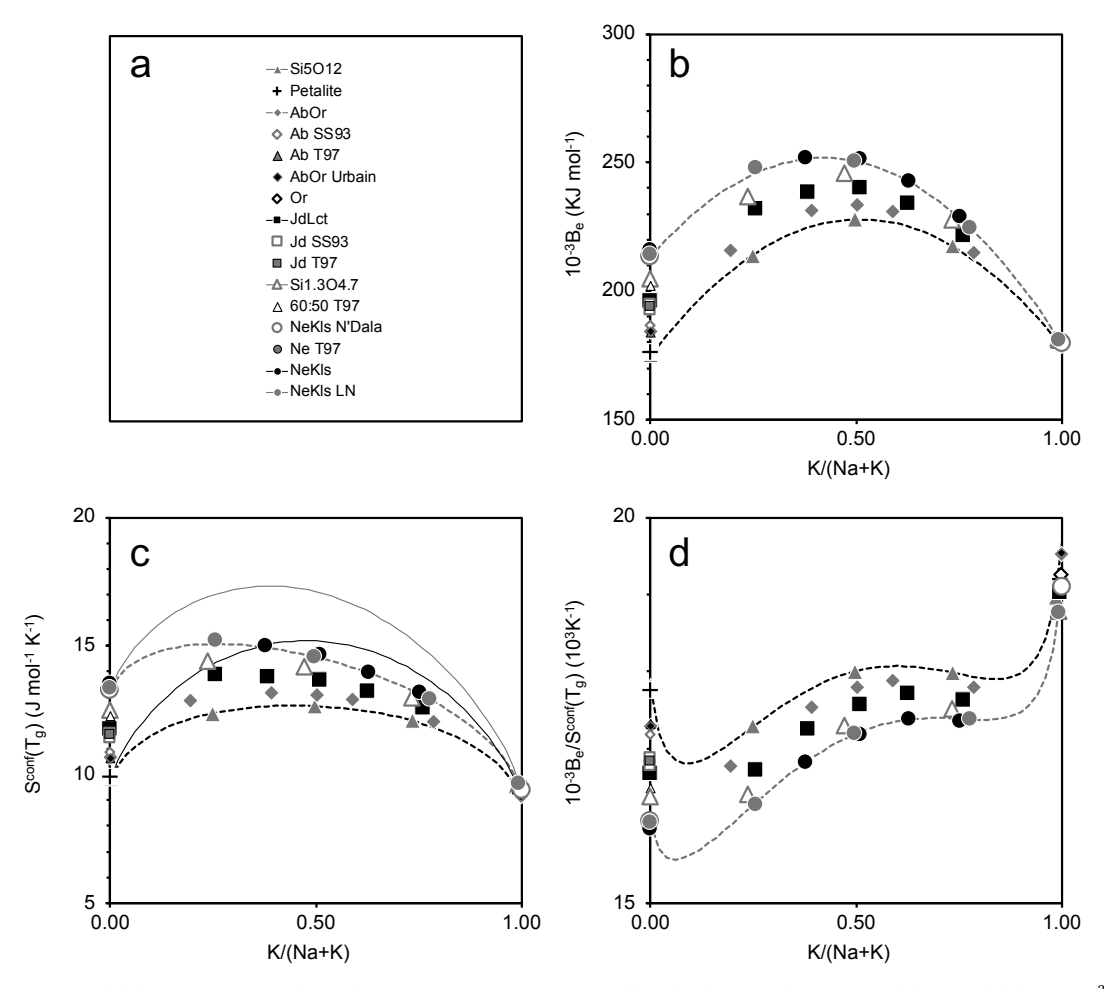


Fig. 10. Global viscosity model for system (Na,K)AlSiO₄, for $A_e = -3.51$ [31]. a. Legend for this figure and Fig. 9. Panels b, c, and d show $10^{-3}B_e$, $S^{conf}(T_g)$, and $10^{-3}B_e/S^{conf}(T_g)$ as a function of X_K , respectively. Black dashed line shows model fo $X_{Al} = 0.17$, grey dashed line for $X_{Al} = 0.5$. Comparison with $S^{conf}(T_g)$ values calculated for ideal mixing is shown in panel c (thin solid lines).

Table 7Fit parameters for the global configurational entropy model.

	$A_e = -3.51$	$A_e = AlSi$
a_1	-3.51	-1.56
a_2	-	-4.93
w_b^{1}	199,715	280,675
w_b^2	32,187	18,470
B_{Na}^{1}	155,049	164,971
B_{Na}^{2}	116,661	27,060
B_K^{-1}	177,611	152,918
B_K^2	3968	76,119
W_s	-10.2	-5.1
c_{Na}^{1}	8.0	10.6
c_{Na}^{1} c_{Na}^{2}	10.5	-0.3
c_K^{-1}	8.9	9.0
c_K^2	1.0	1.0
n	598	598
RMSD	0.32	0.26
Se	0.33	0.27

At constant Al/Si ratio, melt fragility decreases with increasing X_K to be lowest at $X_K = [0.25-0.75]$, then increases again to its highest at $X_K = 1$. The most silicic joins show a "bump" in fragility at K/(Na + K) ratio = 0.5 relative to ratios immediately above or below, also seen as a different slope from the other compositions on the join near the glass transition [18]. The dependence of m on K/(Na + K) ratio parallels that of the $B_e/S^{conf}(T_g)$ ratio. As expected, melts with a higher Al/Si ratio are more fragile (Fig. 13).

5.4. Implications for viscosity models of mixed aluminosilicate melts

We have presented two different families of models based on two different assumptions about the viscosity limit of aluminosilicate melts at very high temperatures. The two different parameterizations show that melt viscosity data in the SiO_2 -(Na,K)AlSiO₄ system can be fitted well, either by keeping A_e constant and allowing $S^{conf}(T_g)$ to vary as a function of Al/Si (in addition to Na/K) ratio, or by allowing A_e to vary as a linear function of Al/Si ratio, in which case $S^{conf}(T_g)$ has only a small dependence on Al/Si ratio.

These global models have a standard error, defined as:

$$Se = \frac{\sum (\eta_{obs} - \eta_{calculated})^2}{(n-f)} = \frac{n(RMSD)^2}{(n-f)},$$
(16)

where n is the number of data and f the number of fit parameters, of 0.33 for the ${A_e}^{-3.51}$ parameterization (12 adjustable parameters) and of 0.27 for the ${A_e}^{AlSi}$ (13 adjustable parameters). Allowing A_e to vary linearly as a function of Al/Si ratio therefore clearly provides a better fit than using a constant $A_e = -3.51$ in the SiO₂-(Na,K)AlSiO₄ system, with only one additional adjustable parameter.

When A_e varies as a linear function of Al/(Al + Si) ratio, there is a spread in B_e as a function of Al/(Al + Si) ratio and only a very small dependence of $S^{conf}(T_g)$ on Al/(Al + Si) ratio (\sim 0.4 J g-atom $^{-1}$ K $^{-1}$ across all Al/(Al + Si) ratios, for all K/(Na + K) ratios; Figs. 9, 11, 14). B_e increases linearly with increasing Al/(Al + Si) ratio; B_e increases at a faster rate for high potassium melts than for high sodium melts (Figs. 9b, 14b). We observe that $S^{conf}(T_g)$ decreases with increasing Al/

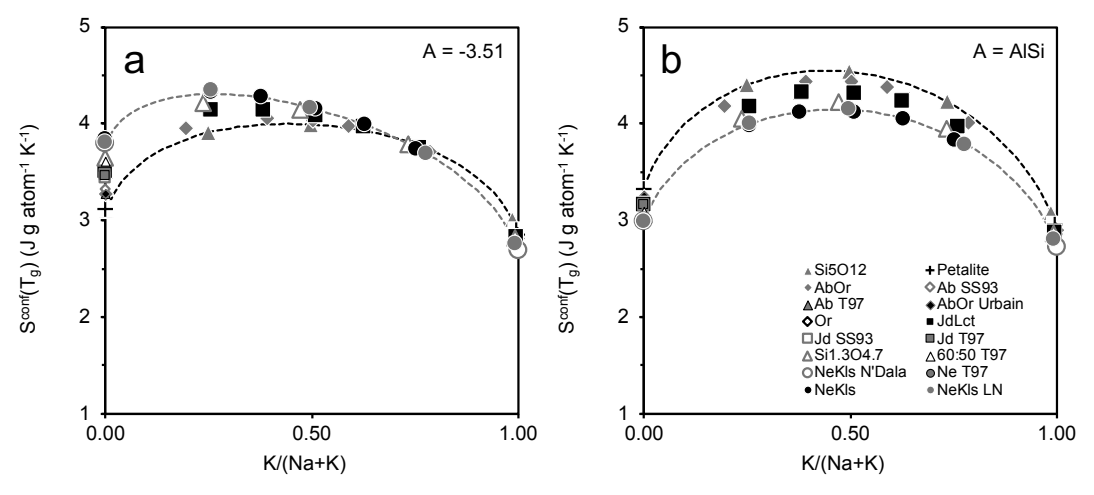


Fig. 11. Configurational entropy at the glass transition in J g-atom⁻¹ K⁻¹. Left panel: $A_e = -3.51$; Right panel: $A_e = 1$ linear function of Al/Si ratio. Black dashed line shows model for $X_{Al} = 0.17$, grey dashed line for $X_{Al} = 0.5$.

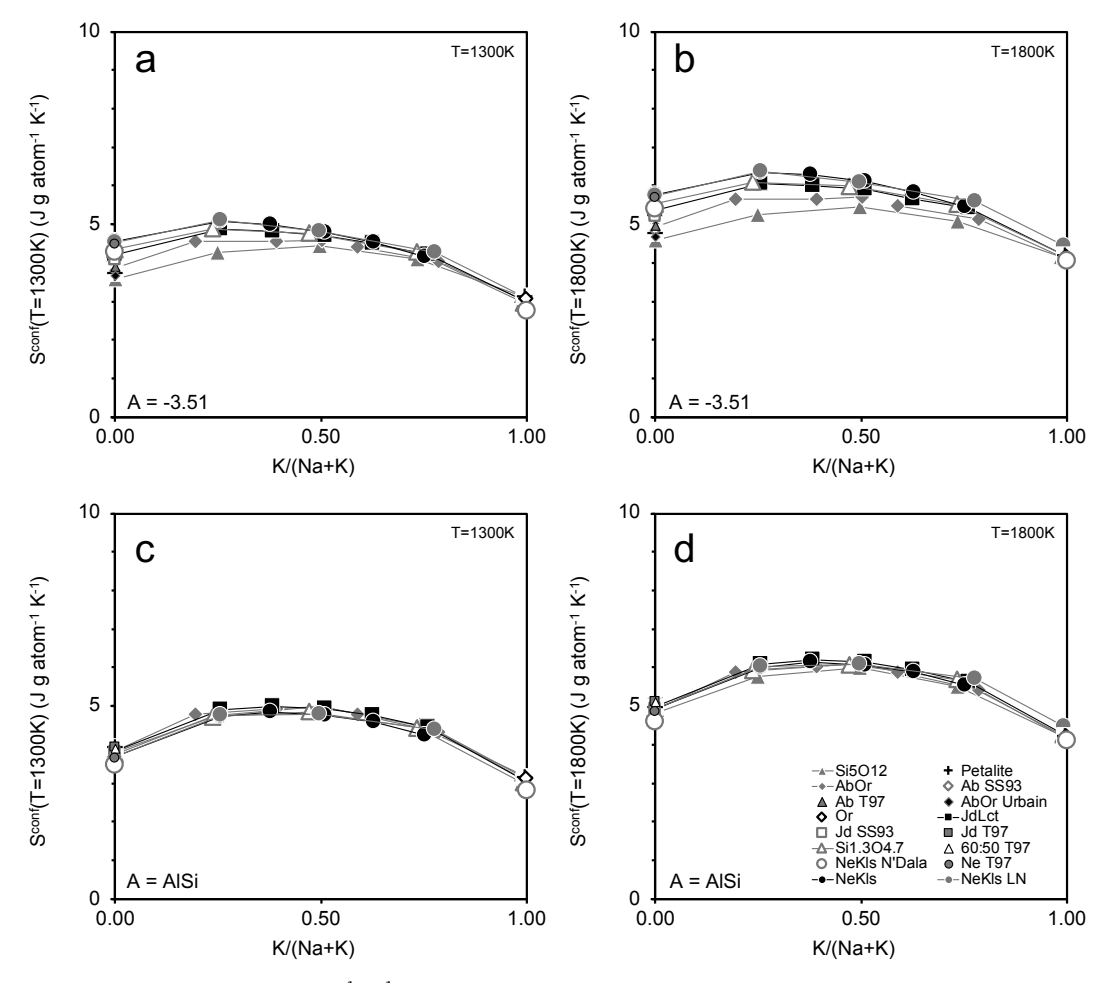


Fig. 12. Isothermal configurational entropy in J g-atom $^{-1}$ K $^{-1}$ calculated at T = 1300 K (left panels) or T = 1800 K (right panels). Top panels: $A_e = -3.51$; Bottom panels: $A_e = 1$ linear function of Al/Si ratio.

(Al + Si) ratio for all K/(Na + K) ratios, with a shallower slope for compositions with Al/(Al + Si) ratio above 0.5 (Fig. 14d). The ratio of $B_e/S^{conf}(T_g)$ increases quasi-linearly with increasing Al/(Al + Si) ratio for all K/(Na + K) ratios; melts with the highest K/(Na + K) ratios see the most dramatic increase. This may be a result of the larger size of the K⁺ cation compared to the Na $^+$ cation. Indeed, for alkali tetrasilicates (M₂Si₄O₉), $B_e/S^{conf}(T_g)$ increases linearly with increasing cation radius

[39].

An increase in the height of the energy barrier to allow configurational changes with increasing Al/(Al + Si) ratio should make configurational changes more difficult. Based solely on this, viscosity may be expected to increase with increasing Al/(Al + Si) ratio. However, our observations are that with increasing Al/(Al + Si) ratio, viscosity decreases, and that with increasing K/(Na + K) ratio, viscosity increases.

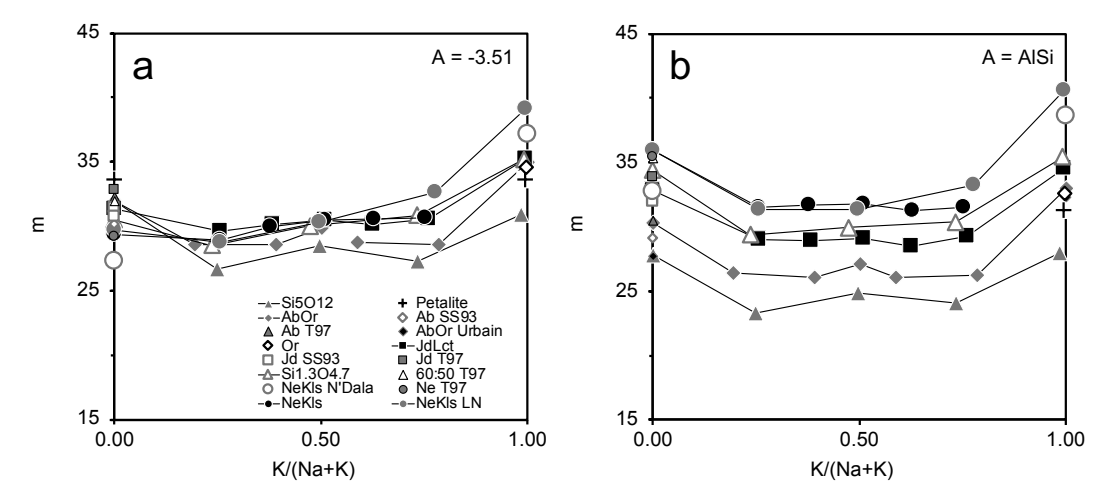


Fig. 13. Fragility as calculated using Eq. 15. Left panel: $A_e = -3.51$; Right panel: $A_e = \text{linear}$ function of Al/Si ratio.

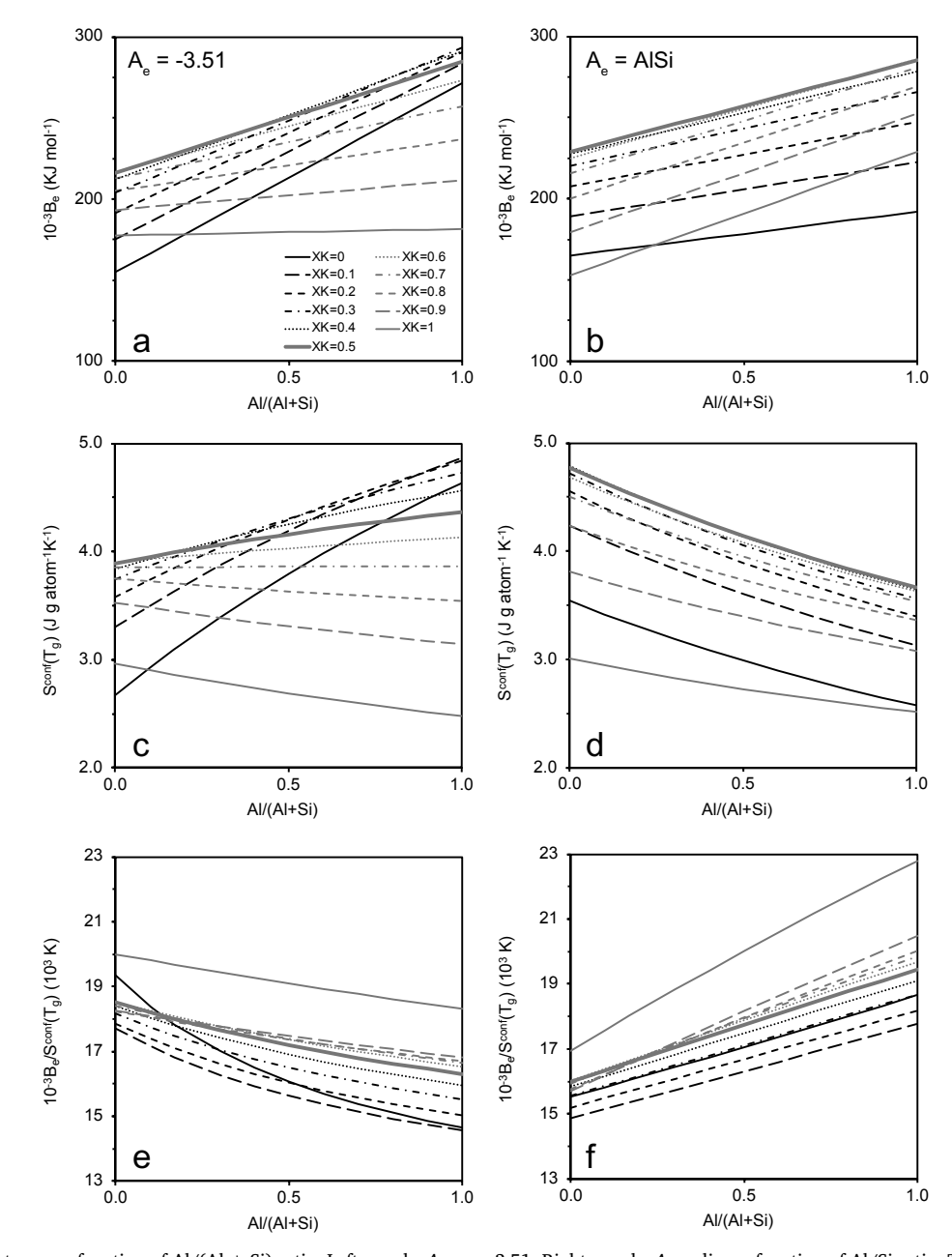


Fig. 14. Model parameters as a function of Al/(Al + Si) ratio. Left panels: $A_e = -3.51$; Right panels: $A_e = \text{linear function of Al/Si ratio. Top: } B_e$, middle: $S^{conf}(T_g)$, and bottom: $10^{-3}B_e/S^{conf}(T_g)$.

Le Losq et al. [19] show that as K replaces Na in a melt at constant Al/ (Al + Si) ratio, it causes the size of tetrahedral cages and rings to increase. This shortens and strengthens the Al-O and Si-O bonds and causes an increase of Al-Al and Al-Si distances. They also show that alkali (Na or K) cluster size increases with increasing Al/(Al + Si) ratio, causing an increase in Al-O-Al linkages. Their molecular dynamics simulations predict Al-O-Al (and therefore Si-O-Si) linkages on the order of 18% for the NeKls join (consistent with NMR studies, e.g., [9]), and on the order of 3% for the AbOr join. Percolation channels in the melt are observed only at high Al/(Al + Si) ratio for high K/(Na + K). Le Losq et al. [19] argue that the segregation of alkali into clusters or channels reduces the mobility of Si, Al, and O, increasing the viscosity of the melts. The model trends in $S^{conf}(T_e)$ and $B_e/S^{conf}(T_g)$ as a function of Al/(Al + Si) ratio may therefore be consistent with an increasing size of the smallest rearranging unit in the melt, z*, caused by alkali clustering at high Al/(Al + Si) ratio, and an associated increase in the height of the energy barrier to configurational changes, $\Delta\mu$. In this parameterization of our global model, the lower viscosity of the NeKls join compared to all other joins in the system is explained by A_e being smaller (more negative) for melts with higher Al/(Al + Si) ratio, reflecting the lower overall bond strength of high Al/(Al + Si) melts because of their greater proportion of Al-O bonds.

6. Summary

The global configurational entropy model for viscosity where A_e is modelled to vary as a linear function of Al/(Al + Si) ratio has a lower RMSD and lower standard error than when A_e is modelled as a constant (Table 7). The better fit obtained by allowing A_e to vary as a function of Al/(Al + Si) ratio is clearly demonstrated in Fig. 8. The variable A_e model is in better agreement with measurements of residual entropy

obtained by calorimetry on congruently melting nepheline, albite, and orthoclase [26], with nepheline having a lower residual entropy than SiO_2 . We argue that the parameters obtained with the variable A_e model are consistent with recent structural data obtained on nominally fully polymerized, mixed Na-K aluminosilicate melts [19], with the implication that the varying A_e accounts for the overall bond strength of the network in the SiO_2 -(Na,K)AlSiO₄ system.

We conclude that the viscosity of nominally fully-polymerized melts in the SiO_2 -(Na,K)AlSiO $_4$ system can be modelled through chemical mixing, without explicit consideration of the important changes in structure related to changes in K/(Na + K) and Al/(Al + Si) ratios. Most of the configurational entropy at the glass transition is a result of Na-K mixing; Si-Al mixing provides little additional contribution.

Acknowledgements

This research was supported by National Science Foundation EAR award 1624321 to G. Robert and EAR award 1724581 to A. Whittington. G. Robert thanks Michael J. Jercinovic at the University of Massachusetts – Amherst for help with electron microprobe analyses, Peter Beach of Bates College for technical support, Bates College undergraduate students Paige Guevarra, Evi Randazzo, and Katherina Tran for help with sample syntheses and characterization, and Alice Doughty for fruitful discussions. G. Robert thanks Anton-Paar for providing viscosity measurements of $Ne_{37.5}$ and Ne_{25} . The authors thank an anonymous reviewer for helpful comments.

Declaration of Competing Interest

None.

Appendix A. Supplementary data

Supplementary data to this article can be found online at https://doi.org/10.1016/j.jnoncrysol.2019.119635.

Appendix A. Appendix

Table A.1 Fit results for the global configurational entropy model.

			$A_e = -3.51$	$A_e = -3.51$									
Suite	$\frac{Al}{Al + Si}$	$\frac{K}{Na+K}$	$A_e^{-3.51}$ (log Pa s)	$10^{-3} B_e^{-3.51}$ (KJ mol ⁻¹)	$S^{conf}(T_g)^{-3.51} (\text{J mol}^{-1} \text{K}^{-1})$	$S^{conf}(T_g)^{-3.51} \text{ (J g atom}^{-1} \text{ K}^{-1})$	$\frac{10^{-3}B_e}{S^{conf}(T_g)}^{-3.51}$ (K)	RMSD Individual					
Si_5O_{12}	0.17	0.00	-3.51	175.2	9.8	3.1	17.8	0.23					
Si_5O_{12}	0.17	0.25	-3.51	213.8	12.4	3.9	17.3	0.57					
Si_5O_{12}	0.17	0.50	-3.51	227.7	12.6	4.0	18.0	0.22					
Si_5O_{12}	0.17	0.73	-3.51	217.4	12.1	3.8	18.0	0.56					
Si_5O_{12}	0.17	0.99	-3.51	181.2	9.6	3.0	19.0	0.28					
Na-petalite T97	0.18	0.00	-3.51	176.1	9.9	3.1	17.8	0.75					
K-petalite	0.22	0.99	-3.51	179.7	9.4	2.9	19.2	0.23					
Ab T97	0.25	0.00	-3.51	183.9	10.6	3.3	17.3	0.40					
Ab SS93	0.27	0.00	-3.51	186.5	10.9	3.3	17.2	0.10					
AbOr	0.25	0.00	-3.51	184.3	10.7	3.3	17.3	0.28					
AbOr	0.25	0.20	-3.51	215.7	12.9	4.0	16.8	0.29					
AbOr	0.25	0.39	-3.51	231.4	13.2	4.1	17.5	0.14					
AbOr	0.25	0.50	-3.51	233.3	13.1	4.0	17.8	0.36					
AbOr	0.25	0.59	-3.51	231.0	12.9	4.0	17.9	0.14					
AbOr	0.25	0.79	-3.51	214.8	12.1	3.7	17.8	0.55					
AbOr	0.25	1.00	-3.51	178.6	9.1	2.8	19.5	0.34					
Or	0.26	1.00	-3.51	179.4	9.3	2.9	19.3	0.25					
Ab Urbain	0.25	0.00	-3.51	184.2	10.6	3.3	17.3	0.12					
Or Urbain	0.25	1.00	-3.51	178.6	9.1	2.8	19.5	0.32					
Jd SS93	0.32	0.00	-3.51	192.7	11.4	3.4	16.9	0.18					
Jd SS93	0.34	0.00	-3.51	195.0	11.6	3.5	16.8	0.16					
Jd T97	0.33	0.00	-3.51	193.9	11.5	3.5	16.8	0.31					
JdLct	0.35	0.00	-3.51	196.1	11.8	3.5	16.7	0.34					

JdLct	0.35	0.26	-3.51	231.6	13.9	4.1	16.7	0.22
JdLct	0.34	0.38	-3.51	238.2	13.8	4.1	17.3	0.32
JdLct	0.35	0.51	-3.51	239.8	13.7	4.1	17.6	0.32
JdLct	0.33	0.63	-3.51	233.8	13.2	4.0	17.7	0.25
JdLct	0.35	0.76	-3.51	221.5	12.6	3.7	17.6	0.41
JdLct	0.35	1.00	-3.51	180.1	9.5	2.8	19.0	0.16
60:50 T97	0.40	0.00	-3.51	202.1	12.3	3.6	16.5	0.23
Si _{1.4} O _{4.7}	0.43	0.00	-3.51	204.7	12.5	3.6	16.4	0.16
$Si_{1.4}O_{4.7}$	0.42	0.24	-3.51	236.8	14.4	4.2	16.4	0.31
$Si_{1.4}O_{4.7}$	0.42	0.47	-3.51	245.6	14.2	4.1	17.3	0.19
$Si_{1.4}O_{4.7}$	0.42	0.73	-3.51	227.6	13.0	3.8	17.5	0.31
$Si_{1.4}O_{4.7}$	0.42	0.99	-3.51	181.1	9.6	2.8	18.8	0.50
Ne T97	0.51	0.00	-3.51	214.3	13.4	3.8	16.0	0.59
NeKls	0.52	0.00	-3.51	215.8	13.5	3.8	16.0	0.50
NeKls	0.52	0.26	-3.51	247.6	15.2	4.3	16.3	0.34
NeKls	0.51	0.38	-3.51	251.8	15.0	4.3	16.8	0.39
NeKls	0.52	0.51	-3.51	251.4	14.6	4.2	17.2	0.69
NeKls	0.50	0.63	-3.51	242.6	14.0	4.0	17.4	0.32
NeKls	0.52	0.75	-3.51	228.9	13.2	3.7	17.4	0.38
NeKls LN	0.51	0.00	-3.51	214.1	13.3	3.8	16.0	0.41
NeKls LN	0.52	0.26	-3.51	247.6	15.2	4.3	16.3	0.22
NeKls LN	0.50	0.50	-3.51	250.4	14.6	4.2	17.2	0.15
NeKls LN	0.50	0.78	-3.51	224.5	12.9	3.7	17.4	0.07
NeKls LN	0.50	0.99	-3.51	180.9	9.6	2.8	18.8	0.17
Ne Ndala	0.50	0.00	-3.51	213.4	13.3	3.8	16.1	0.15
Kls Ndala	0.50	1.00	-3.51	179.6	9.4	2.7	19.1	0.04
HPG8	0.16	0.38	-3.51	223.3	12.6	4.0	17.8	0.32

	$\underline{A_e = -3.51}$	$A_e = AlSi$									
Suite	RMSD Join	A _e ^{AlSi} (log Pa s)	$10^{-3} B_e^{AlSi}$ (KJ mol ⁻¹)	$S^{conf}(T_g)^{AlSi}$ (J mol ⁻¹ K ⁻¹)	$S^{conf}(T_g)^{AlSi}$ (J g atom ⁻¹ K ⁻¹)	$\frac{10^{-3}B_{\ell}}{S^{conf}(T_g)}^{AlSi} \text{ (K)}$	RMSD Individual	RMSD Join			
Si_5O_{12}	0.39	-2.41	169.6	10.6	3.3	16.0	0.27	0.38			
Si_5O_{12}		-2.38	221.6	13.9	4.4	15.9	0.55				
Si_5O_{12}		-2.39	238.6	14.4	4.5	16.6	0.14				
Si_5O_{12}		-2.39	222.1	13.4	4.2	16.6	0.50				
Si_5O_{12}		-2.41	170.1	9.8	3.1	17.4	0.40				
Na-petalite T97		-2.45	169.9	10.6	3.3	16.1	0.29				
K-petalite		-2.67	171.6	9.5	3.0	18.0	0.18				
Ab T97		-2.78	171.7	10.5	3.2	16.3	0.16				
Ab SS93		-2.89	172.3	10.5	3.2	16.3	0.15				
AbOr	0.31	-2.79	171.8	10.5	3.2	16.3	0.15	0.25			
AbOr		-2.79	216.6	13.6	4.2	15.9	0.21				
AbOr		-2.78	239.8	14.4	4.4	16.6	0.05				
AbOr		-2.79	243.1	14.4	4.4	16.9	0.35				
AbOr		-2.77	240.7	14.2	4.4	16.9	0.06				
AbOr		-2.79	219.9	13.0	4.0	16.9	0.51				
AbOr		-2.81	172.2	9.3	2.9	18.5	0.26				
Or		-2.84	173.7	9.5	2.9	18.3	0.19				
Ab Urbain		-2.79	171.7	10.5	3.2	16.3	0.19				
Or Urbain		-2.79 -2.79	171.7	9.3	2.9	18.5	0.69				
Jd SS93		-3.15	173.7	10.5	3.2	16.5	0.17				
Jd SS93					3.1	16.6					
		-3.25	174.2	10.5			0.12				
Jd T97	0.00	-3.20	174.0	10.5	3.2	16.5	0.31	0.05			
JdLct	0.29	-3.28	174.8	10.6	3.2	16.5	0.37	0.25			
JdLct		-3.28	230.3	14.0	4.2	16.5	0.16				
JdLct		-3.22	243.6	14.4	4.3	16.9	0.25				
JdLct		-3.27	248.7	14.4	4.3	17.2	0.33				
JdLct		-3.21	243.8	14.1	4.2	17.3	0.12				
JdLct		-3.31	230.7	13.3	4.0	17.3	0.30				
JdLct		-3.29	181.0	9.6	2.9	18.8	0.12				
60:50 T97		-3.55	175.9	10.5	3.1	16.8	0.28				
Si _{1.4} O _{4.7}	0.31	-3.66	176.5	10.5	3.1	16.8	0.03	0.26			
Si _{1.4} O _{4.7}		-3.64	230.4	13.9	4.0	16.6	0.29				
Si _{1.4} O _{4.7}		-3.64	252.4	14.5	4.2	17.4	0.17				
Si _{1.4} O _{4.7}		-3.64	239.1	13.6	4.0	17.6	0.32				
Si _{1.4} O _{4.7}		-3.62	187.0	9.8	2.9	19.1	0.39				
Ne T97		-4.06	178.7	10.5	3.0	17.1	0.10				
NeKls	0.37	-4.12	179.3	10.5	3.0	17.1	0.15	0.19			
NeKls		-4.11	237.9	14.0	4.0	17.0	0.12				
NeKls		-4.05	251.6	14.4	4.1	17.4	0.19				
NeKls		-4.12	258.5	14.5	4.1	17.8	0.20				
NeKls		-4.04	254.2	14.2	4.0	17.9	0.20				
NeKls		-4.12	243.2	13.5	3.8	18.0	0.37				

NeKls LN	0.25	-4.05	178.7	10.5	3.0	17.1	0.14	0.18
NeKls LN		-4.11	237.9	14.0	4.0	17.0	0.19	
NeKls LN		-4.02	257.1	14.5	4.1	17.7	0.08	
NeKls LN		-4.04	238.5	13.3	3.8	18.0	0.10	
NeKls LN		-4.01	192.2	9.8	2.8	19.6	0.37	
Ne Ndala		-4.02	178.5	10.5	3.0	17.1	0.51	
Kls Ndala		-4.02	191.0	9.5	2.7	20.0	0.19	
HPG8		-2.34	234.1	14.4	4.6	16.3	0.42	

References

- G. Adam, J. Gibbs, On the temperature dependence of cooperative relaxation properties in glass-forming liquids, J. Chem. Phys. 43 (1965) 139–146.
- [2] J.R. Allwardt, J.F. Stebbins, Ca-Mg and K-Mg mixing around non-bridging O atoms in silicate glasses: an investigation using ¹⁷O MAS and 3QMAS NMR, Am. Mineral. 89 (2004) 777-784.
- [3] I. Avramov, A. Milchev, Effect of disorder on diffusion and viscosity in condensed systems, J. Non-Cryst. Solids 104 (1988) 253–260.
- [4] M. Bouhifd, A. Sipp, P. Richet, Heat capacity, viscosity, and configurational entropy of alkali titanosilicate melts, Geochim. Cosmochim. Acta 63 (1999) 2429–2437.
- [5] M. Davis, The effect of water on the viscosity of silicate melts: a configurational entropy approach, Geochim. Cosmochim. Acta 63 (2) (1999) 167–173.
- [6] D.E. Day, Mixed alkali glasses their properties and uses, J. Non-Cryst. Solids 21 (1976) 343–372.
- [7] D. Dingwell, N. Bagdassarov, G. Bussod, S. Webb, Magma rheology, in: R.W. Luth (Ed.), Short Course Handbook on Experiments at High Pressure and Applications to the Earth's Mantle, vol. 21, Mineralogical Association of Canada, Edmonton, Alberta, 1993, pp. 131–196.
- [8] D. Dingwell, S. Webb, Relaxation in silicate melts, Eur. J. Mineral. 2 (1990) 427–449.
- [9] E.V. Dubinsky, J. Stebbins, Quench rate and temperature effects on framework ordering in aluminosilicate melts, Am. Mineral. 91 (5-6) (2006) 753-761.
- [10] J.M. Getson, A.G. Whittington, Liquid and magma viscosity in the anorthite-forsterite-diopside-quartz system and implications for the viscosity-temperature paths of cooling magmas, J. Geophys. Res. 112 (B10) (2007) (19pp).
- [11] G.N. Greaves, EXAFS and the structure of glass, J. Non-Cryst. Solids 71 (1985)
- [12] G.N. Greaves, K.L. Ngai, Reconciling ionic-transport properties with atomic structure in oxide glasses, Phys. Rev. B 52 (9) (1995) 6358–6380.
- [13] F. Holtz, H. Behrens, D. Dingwell, R. Taylor, Water solubility in aluminosilicate melts of haplogranite composition at 2 kbar, Chem. Geol. 96 (1992) 289–302.
- [14] J.O. Isard, The mixed alkali effect in glass, J. Non-Cryst. Solids 1 (1969) 235–261.
- [15] K.D. Kim, S.-H. Lee, Viscosity behavior and mixed alkali effect of alkali aluminosilicate glass melts, J. Ceram. Soc. Jpn. 105 (1997) 827–832.
- [16] R. Knoche, D.B. Dingwell, F.A. Seifert, S.L. Webb, Non-linear properties of supercooled liquids in the system Na₂O-SiO₂, Chem. Geol. 116 (1994) 1–16.
- [17] R.A. Lange, A revised model for the density and thermal expansivity of K₂O-Na₂O-CaO-MgO-Al₂O₃-SiO₂ liquids from 700 to 1900 K: extension to crustal magmatic temperatures, Contrib. Mineral. Petrol. 130 (1) (1997) 1–11.
- [18] C. Le Losq, D. Neuville, Effect of the Na/K mixing on the structure and the rheology of tectosilicate silica-rich melts, Chem. Geol. 346 (2013) 57–71.
- [19] C. Le Losq, D.R. Neuville, W. Chen, P. Florian, D. Massiot, Z. Zhou, G.N. Greaves, Percolation channels: a universal idea to describe the atomic structure and dynamics of glasses and melts, Sci. Rep. 7 (2017) 1–12.
- [20] S.K. Lee, J.F. Stebbins, Effects of the degree of polymerization on the structure of sodium silicate and aluminosilicate glasses and melts: an ¹⁷O NMR study, Geochim. Cosmochim. Acta 73 (4) (2009) 1109–1119.
- [21] W. Loewenstein, The distribution of aluminum in the tetrahedra of silicates and aluminates, Am. Mineral. 39 (1954) 92–96.
- [22] J.C. Mauro, Y. Yue, A.J. Ellison, P.K. Gupta, D.C. Allan, Viscosity of glass-forming

- liquids, Proc. Natl. Acad. Sci. 106 (47) (2009) 19780-19784.
- [23] J.B. Murdoch, J.F. Stebbins, I.S.E. Carmichael, High-resolution ²⁹Si NMR study of silicate and aluminosilicate glasses: the effect of network-modifying cations, Am. Mineral. 70 (1985) 332–343.
- [24] I. N'dala, F. Cambier, M.R. Anseau, G. Urbain, Viscosity of liquid feldspars part I: viscosity measurements, Trans. J. Br. Ceram. Soc. 83 (1984) 105–107.
- [25] D. Neuville, P. Richet, Viscosity and mixing in molten (Ca, Mg) pyroxenes and garnets, Geochim. Cosmochim. Acta 55 (4) (1991) 1011–1019.
- [26] P. Richet, Viscosity and configurational entropy of silicate melts, Geochim. Cosmochim. Acta 48 (1984) 471–483.
- [27] P. Richet, Heat capacity of silicate glasses, Chem. Geol. 62 (1987) 111-124.
- [28] P. Richet, Y. Bottinga, Glass transitions and thermodynamic properties of amorphous SiO₂, NaAlSi_nO_{2n+2} and KAlSi₃O₈, Geochim. Cosmochim. Acta 48 (3) (1984) 453–470.
- [29] P. Richet, R. Robie, B. Hemingway, Low-temperature heat capacity of diopside glass (CaMgSi₂O₆): a calorimetric test of the configurational-entropy theory applied to the viscosity of liquid silicates, Geochim. Cosmochim. Acta 50 (1986) 1521–1533.
- [30] E.F. Riebling, Structure of sodium aluminosilicate melts containing at least 50 mole % SiO₂ at 1500°C, J. Chem. Phys. 44 (8) (1966) 2857–2865.
- [31] J.K. Russell, D. Giordano, Modelling configurational entropy of silicate melts, Chem. Geol. 461 (2017) 140–151.
- [32] J.K. Russell, D. Giordano, D.B. Dingwell, High-temperature limits on viscosity of non-Arrhenian silicate melts, Am. Mineral. 88 (8–9) (2003) 1390–1394.
- [33] A.G. Ryan, J.K. Russell, A.R.L. Nichols, K.-U. Hess, L.A. Porritt, Experiments and models on H₂O retrograde solubility in volcanic systems, Am. Mineral. 100 (4) (2015) 774–786.
- [34] S.K. Sharma, D. Virgo, B.O. Mysen, Raman study of the coordination of aluminum in jadeite melts as a function of pressure, Am. Mineral. 64 (1979) 779–787.
- [35] J.F. Stebbins, I.S.E. Carmichael, L.K. Moret, Heat capacities and entropies of silicate liquids and glasses, Contrib. Mineral. Petrol. 86 (1984) 131–148.
- [36] J.F. Stebbins, Z. Xu, NMR evidence for excess non-bridging oxygen in an aluminosilicate glass, Nature 390 (1997) 60–62.
- [37] D.J. Stein, F.J. Spera, Experimental rheometry of melts and supercooled liquids in the system NaAlSiO₄-SiO₂: implications for stucture and dynamics, Am. Mineral. 78 (1993) 710–723.
- [38] T.D. Taylor, G.E. Rindone, Properties of soda aluminosilicate glasses: V, low-temperature viscosities, J. Am. Ceram. Soc. 53 (12) (1970) 692–695.
- [39] M.J. Toplis, Energy barriers to viscous flow and the prediction of glass transition temperatures of molten silicates, Am. Mineral. 83 (5–6) (1998) 480–490.
- [40] M.J. Toplis, D.B. Dingwell, K. Hess, T. Lenci, Viscosity, fragility, and configurational entropy of melts along the join SiO₂-NaAlSiO₄, Am. Mineral. 82 (1997) 979–990.
- [41] M.J. Toplis, D.B. Dingwell, T. Lenci, Peraluminous viscosity maxima in Na₂O-Al₂O₃-SiO₂ liquids: the role of triclusters in tectosilicate melts, Geochim. Cosmochim. Acta 61 (1997) 2605–2612.
- [42] G. Urbain, Y. Bottinga, P. Richet, Viscosity of liquid silica, silicates and aluminosilicates, Geochim. Cosmochim. Acta 46 (1982) 1016–1072.
- [43] H. Vogel, Das Temperaturabhängigkeitsgesetz der Viscosität von Flüssigkeiten, Physik Zeitschr XXII (1921) 645-646
- [44] G. Wu, E. Yazhenskikh, K. Hack, E. Wosch, M. Müller, Viscosity model for oxide melts relevant to fuel slags. Part 1: pure oxides and binary systems in the system SiO₂–Al₂O₃–CaO–MgO–Na₂O–K₂O, Fuel Process. Technol. 137 (C) (2015) 93–103.